

Characterizing regional oceanography and bottom environmental conditions at two contrasting sponge grounds on the northern Labrador Shelf.

5 Evert de Froe^{1,2,3*}, Igor Yashayaev⁴, Christian Mohn⁵, Johanne Vad⁶, Furu Mienis¹, Gerard Duineveld¹, Ellen Kenchington⁴, Erica Head⁴, Steve W. Ross⁷, Sabena Blackbird⁸, George A. Wolff⁸, J. Murray Roberts⁶, Barry MacDonald⁴, Graham Tulloch⁹, Dick van Oevelen¹⁰

10 ¹ NIOZ Royal Netherlands Institute for Sea Research, Department of Ocean Systems, PO Box 59, 1790 AB, Den Burg, the Netherlands

² Centre for Fisheries Ecosystems Research, Fisheries and Marine Institute of Memorial University of Newfoundland and Labrador, St. John's, Newfoundland and Labrador, Canada

³ Wageningen Marine Research, Wageningen University and Research, PO Box 77, 4400 AB Yerseke, the Netherlands

⁴ Bedford Institute of Oceanography, Department of Fisheries and Oceans, PO Box 1006, Dartmouth, NS, Canada B2Y 4A2

15 ⁵ Department of Ecoscience, Aarhus University, Frederiksborgvej 399, 4000 Roskilde, Denmark

⁶ Changing Oceans Research Group, School of GeoSciences, The University of Edinburgh, Edinburgh, United Kingdom

⁷ Univ. of North Carolina at Wilmington, Center for Marine Science, 5600 Marvin Moss Ln., Wilmington, NC, 28409 USA

⁸ School of Environmental Sciences, University of Liverpool, 4 Brownlow Street, Liverpool, L69 3GP, UK.

⁹ British Geological Survey, Lyell Centre, Research Avenue South, Edinburgh, EH14 4AP

20 ¹⁰ NIOZ Royal Netherlands Institute for Sea Research, Department of Estuarine and Delta Systems, PO Box 140, 4400 AC, Yerseke, the Netherlands

Correspondence to: Evert de Froe (evert.defroe@wur.nl)

Abstract. Deep-sea sponge grounds are distributed globally and are considered hotspots of biological diversity and biogeochemical cycling. To date, little is known about the environmental conditions that allow high sponge biomass to develop in the deep sea. Here, we characterize oceanographic conditions at two contrasting sites off the northern Labrador Shelf with high- and low-sponge-biomass. Data were collected by year-long benthic lander deployments equipped with current meters, a turbidity and chlorophyll-*a* measuring device, and a sediment trap. Additionally, regional oceanography was described by analyzing vertical conductivity-temperature-depth (CTD) casts, Argo float profiles, and surface buoy drifter data for the northern Labrador Shelf from 2005 to 2022. Stable isotopic composition of benthic fauna was determined to investigate food web structure at the sponge grounds. Our results revealed strong ($0.26 \pm 0.14 \text{ m s}^{-1}$; mean \pm SD) semidiurnal tidal currents at the high-sponge-biomass site, but twofold weaker currents ($0.14 \pm 0.08 \text{ m s}^{-1}$; mean \pm SD) at the low-sponge-biomass site. Tidal analysis suggests that, at the high-sponge-biomass site, kinetic energy is dissipated from barotropic tide to baroclinic tide/turbulence, which could enhance food availability for benthic organisms. Bottom nutrient concentrations were elevated at the high-sponge-biomass site which would benefit growth in deep-sea sponges. Organic matter flux to the seafloor was increased at the high-sponge-biomass site and consisted of fresher material. Finally, both sponge grounds demonstrated tight

benthic-pelagic coupling prior to the onset of stratification. Stable isotope signatures indicated that soft corals (*Primnoa resedaeformis*) fed on suspended particulate organic matter, while massive sponges (*Geodia* spp.) likely utilized additional food sources. Our results imply that benthic fauna at the high-sponge-biomass site benefit from strong tidal currents, which increases food supply, and favourable regional ocean currents that increase nutrient concentration in bottom waters.

40 1 1 Introduction

Sponges are an ancient group of sessile filter feeders capable of pumping large quantities of water through their bodies (Bergquist, 1978; Leys et al., 2011; Vogel, 1977), thereby exchanging significant amounts of particulate- and dissolved organic matter and nutrients with the water column (e.g., van Duyl et al., 2008; Maldonado et al., 2012; Kahn et al., 2015; Rix et al., 2016). In the deep sea, sponges can form dense aggregations, known as sponge grounds, which are considered hotspots of
45 macrofaunal diversity and abundance (Beazley et al., 2013; Buhl-Mortensen et al., 2010; Klitgaard, 1995; McIntyre et al., 2016), carbon- and nutrient cycling (Cathalot et al., 2015; Kutti et al., 2013; Maldonado et al., 2020b), and benthic-pelagic coupling (Pile and Young, 2006). Sponge grounds form complex habitats that provide breeding grounds and shelter for (commercially important) fish, increasing demersal fish biomass and diversity (Brodnicke et al., 2023; Kenchington et al., 2013; Kutti et al., 2015; Meyer et al., 2019). Finally, they are often classified as Vulnerable Marine Ecosystems (VMEs) as
50 defined by the Food and Agriculture Organization of the United Nations (FAO, 2009).

Deep-sea sponge ecosystems are currently under threat from anthropogenic disturbances such as deep-water bottom trawling, deep-sea mining, and climate change. Pham et al. (2019) found that large quantities of sponges (~4% of total stock) have been removed by bottom trawling from sponge grounds on the Flemish Cap. Deep-sea sponges are especially vulnerable to bottom
55 fishing due their longevity and slow growth (Hogg et al., 2010; Leys and Lauzon, 1998). Benthic trawling reduces the density and diversity of deep-sea sponge grounds (Colaço et al., 2022; Morrison et al., 2020), and recovery of disturbed sponge habitats can take decades to centuries (Vieira et al., 2020). In addition, prolonged exposure to elevated concentrations of suspended sediments, e.g. due to deep-sea mining, could adversely affect deep-sea sponges (Wurz et al., 2021). Recent studies suggest that climate change also impacts deep-sea benthic fauna (Brito-Morales et al., 2020; Jorda et al., 2020). For example, modelling
60 predicted that the suitable area for *Vazella pourtalesii* on the Scotian Shelf would increase four-fold in the coming years due to warming of colder waters around its current habitat (Beazley et al., 2021). Nevertheless, research on the effect of climate change on deep-sea sponges is still in its infancy and to predict its effects on sponge grounds, a better understanding of the environmental conditions that favour their occurrence is needed.

65 In the past decades, research on deep-sea sponges has focused on their physiology and feeding behaviour (e.g., Leys and Lauzon, 1998; Yahel et al., 2007; Kahn et al., 2015; Robertson et al., 2017; Kazanidis et al., 2018; Maier et al., 2020b; Bart et al., 2021; de Kluijver et al., 2021), and assessing their spatial distributions using habitat suitability models (Beazley et al.,

2018; Howell et al., 2016; Knudby et al., 2013; Murillo et al., 2018). More recently, data on the environmental conditions where sponge grounds are found have been gathered using long-term measurements from lander-mounted equipment. These data indicate that sponge grounds are commonly found in areas with internal waves (Davison et al., 2019) and comparatively strong tidal currents which flush the seafloor with oxygen and nutrient-rich water, and with a high suspended particle matter load near the seabed (Hanz et al., 2021b, a; Roberts et al., 2018). In addition, sponges can alter the hydrodynamic conditions of the benthic boundary layer by increasing the bottom roughness, creating conditions favourable for larval recruitment and suspended particle deposition (Abelson and Denny, 1997; Culwick et al., 2020). These studies show that sponge grounds are found in areas with a variety of environmental conditions, but little is known of the mechanisms controlling their spatial distribution or what controls their biomass.

The Canadian Atlantic continental shelf breaks and upper slopes, including the northern Labrador Shelf, host extensive sponge grounds (Kenchington et al., 2010; Knudby et al., 2013). Sponge assemblages occur over a large depth range (200 – 2875 m) and are often aligned along depth contours with presumably similar environmental conditions (Murillo et al., 2012; Knudby et al., 2013). On the northern Labrador Shelf and upper slope, sponge assemblages consist mostly of *Geodia* spp. and glass (hexactinellid) sponges (Kenchington et al., 2010) but with locally variable sponge biomass. Therefore, this region provides a suitable setting to study which environmental conditions favour high sponge biomass and to provide insight into the factors that drive the spatial distribution of sponge assemblages on the eastern Canadian Shelf. Furthermore, research on present environmental conditions on the seafloor is timely as the Labrador Shelf region is one of the fastest warming large marine ecosystems globally (~ 1 °C decade⁻¹; Belkin, 2009), and according to ensemble-based climate change prediction, critical water mass properties there, including temperature, particulate organic carbon, pH, and aragonite saturation, are likely to change substantially by 2100 (Puerta et al., 2020). Recent work on the Labrador Sea also shows that Arctic sea-ice melt can impact the hydrographic conditions in this region (Yashayaev, 2024). Therefore, analysis of the contemporary conditions provides a baseline or a benchmark for referencing future ocean and ecosystem conditions. This study presents a valuable reference dataset for the upper slope of the northern Labrador Shelf against which future changes could be evaluated.

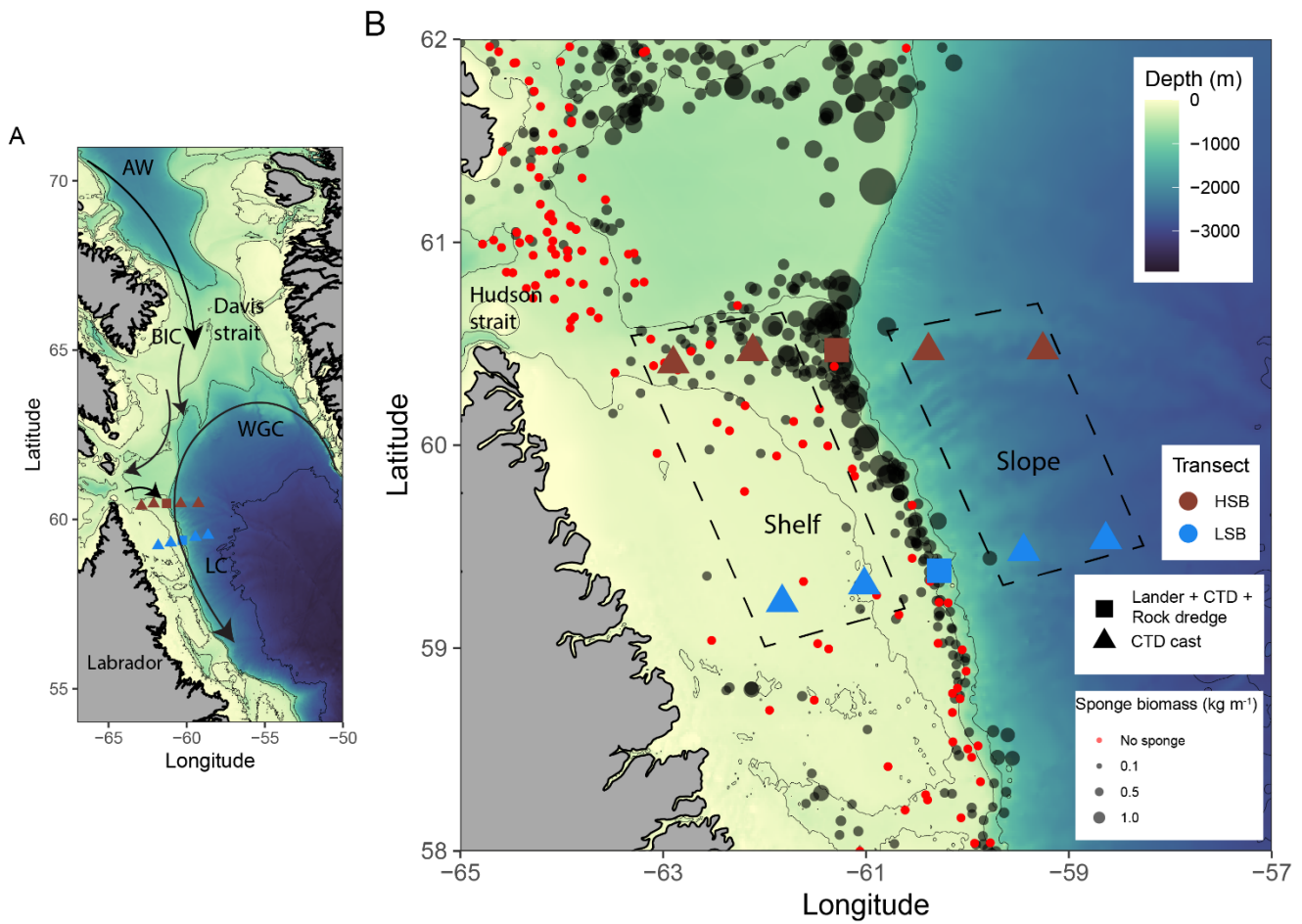
To obtain a better understanding of the environmental conditions and ecosystem functioning of high- and low-sponge-biomass sites on the upper slope of the northern Labrador Shelf, this study specifically aimed to examine: (i) differences in ocean dynamics and seawater properties, (ii) the annual dynamics of near-bed environmental and hydrodynamic conditions, and (iii) differences in organic matter flux and isotopic signatures for sponges and associated macrofauna. To this end, data on regional oceanography of the Northern Labrador Shelf was collected from CTD casts, Argo float profiles, and surface drifter buoys. Bottom hydrodynamic- and environmental conditions were assessed using two year-long benthic lander deployments. Organic matter fluxes were measured with sediment traps, and benthic macrofauna was sampled by two rock dredge deployments. This study is the first to collect year-long hydrodynamic and environmental data simultaneously at a high- and a low-biomass sponge ground.

2 Material and methods

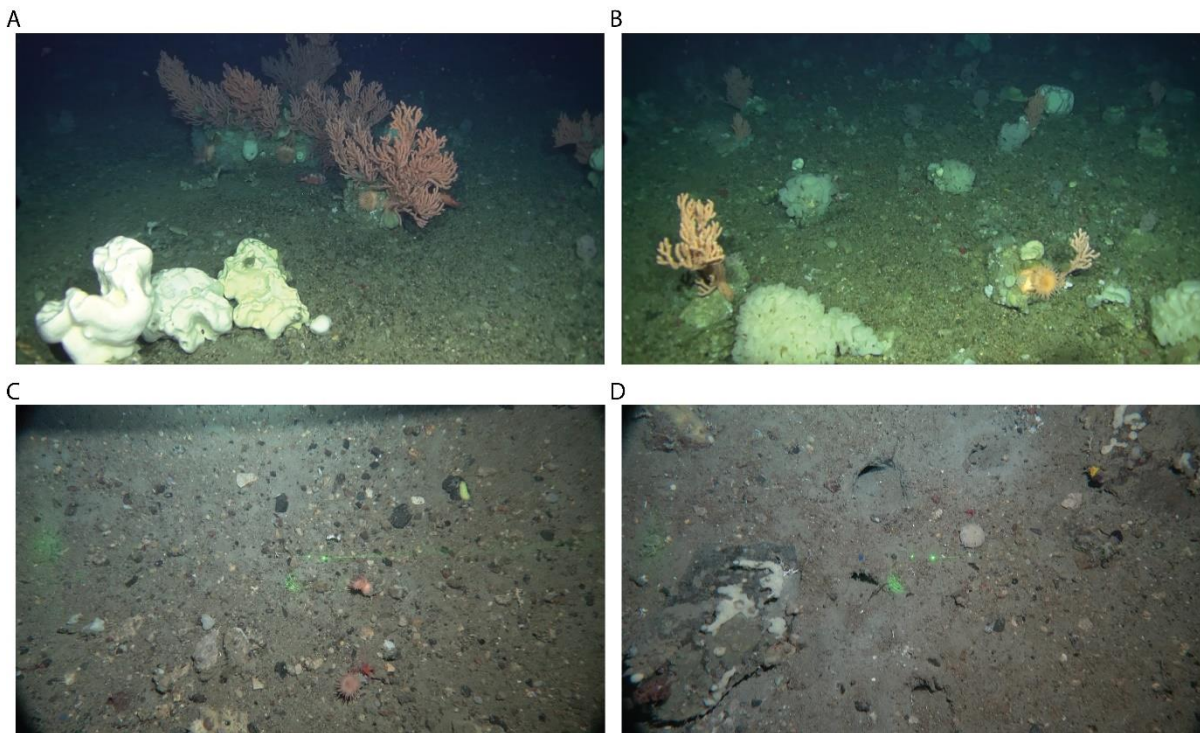
2.1 Oceanographic setting and the study area

The study area comprises the northern Labrador Shelf and upper slope and extends from the south-eastern Hudson Strait outflow region to the base of the Labrador slope (Fig. 1A). This region is known for intense mixing and water mass transformation (Dunbar, 1951; Kollmeyer et al., 1967; Griffiths et al., 1981; Drinkwater and Jones, 1987) and four distinct flow components can be identified (Fig. 1A; Smith et al., 1937; Yashayaev, 2007; Straneo and Saucier, 2008; Curry et al., 2011, 2014): first, the cold and relatively fresh Arctic outflow, passing through the Davis Strait via the Baffin Island Current (BIC), enters the region from the north as Arctic Water (AW) and Baffin Bay Water (BBW; Sherwood et al., 2021); second, the West Greenland Current (WGC) approaches our study site from the northeast; third, Irminger Water (IW), a warmer and saltier water mass, can often be seen below the WGC, usually >150 m depth; and fourth, Hudson Strait outflow water which enters the region from the west. The resulting aggregated boundary current joins the Labrador Current (LC) flowing southward along the Labrador Shelf/slope, effectively forming and maintaining a baroclinic transition between the less-saline shelf water and the more-saline deep-basin water (Yashayaev, 2007).

The northern Labrador Shelf hosts multiple sponge grounds with contrasting sponge community composition, density, and biomass (Dinn et al., 2020; Kenchington et al., 2010). We selected a high-sponge-biomass site (HSB; 410 m depth) in the north and a low-sponge-biomass site (LSB; 558 m depth) in the south of the study area (Table S1; Fig. 1B), approximately 130 km apart. The substrate at the HSB lander location consisted mostly of pebbles, cobbles, and boulders (Fig. 2 A & B; Kenchington et al., 2010; Dinn et al., 2020) and a visual assessment of the sediment type at the LSB lander location suggested the dominance of gravel (Coté et al., 2019). The seafloor at the HSB lander was characterized by large-sized massive demosponges (e.g. *Geodia* spp.), glass sponges (e.g. *Asconema* spp.), and large gorgonian corals (*Primnoa resedaeformis*; Fig. 2 A & B; Kenchington et al., 2010; Dinn et al., 2020). The benthic community at LSB consisted mostly of small specimens of corals including *Anthomastus* sp., as well sponges as *Polymastia* sp., *Craniella* sp., *Axinella* sp., and possibly *Mycale* sp. (Fig. 2 C & D; Coté et al., 2019). The HSB lander was located on the shelf on a 2° slope and slope aspect was directed northwest at 60°. The LSB lander was located on the upper slope, east of the shelf break, on a 7° slope and aspect was directed southeast at 105° (Fig. S1).



130 **Figure 1: Map of the study area with (A) the general circulation pattern (Curry et al., 2014). Cold Arctic Water (AW) flows southward**
through the Davis Strait and continues as the surface-intensified Baffin Island Current. The warmer, more saline West Greenland
Slope Current (WGC) of North Atlantic origin largely follows the continental slope in the depth range 150 – 800 m and is deflected
westward at approximately 64° N. Cold and fresh water leaves Hudson Strait and joins the BIC and WGC to form the offshore
135 **branch of the Labrador Current (Straneo and Saucier, 2008). (B) Location of lander deployments and CTD-casts, with sponge**
biomass (in kg m⁻¹) based on Kenchington et al. (2010). Dotted line boxes indicate the shallow shelf and deeper slope stations at both
sites. HSB = high-sponge-biomass transect (red symbols), LSB = low-sponge-biomass transect (blue symbols).



140 **Figure 2: Images of benthic lander deployment sites, at the high-sponge-biomass lander site (HSB; A,B) and low-sponge-biomass lander site (LSB; C, D). ROV image credits: ArcticNet/Canadian Scientific Submersible Facility (CSSF)/Department of Fisheries and Oceans (DFO). Laser points in panel C & D are 6 cm apart.**

2.2 Sampling methodology

2.2.1 Near-bed lander deployment

145 Landers were deployed during research cruise Amundsen 2018 leg 2c (27 July 2018) and retrieved during research cruise Amundsen 2019 leg 1b (1 & 2 July 2019). The landers were each equipped with a 2 MHz single point measurement ADCP (upward-looking, Nortek Aquadopp), a sediment trap, and a combined optical backscatter sensor (OBS) for turbidity and fluorescence (Wetlabs ECO-FLNTU; Table S1).

150 The ADCPs collected data on pressure, water velocity, echo intensity (ABS; acoustic backscatter signal), and water temperature at a 10 minute interval. Furthermore, the built-in accelerometer and magnetometer in the ADCPs collected data on heading, pitch, and roll. The ADCP was mounted 2 m above the bottom, the blanking distance was 1.14 m. Velocity data were recorded in beam coordinates and transformed in MATLAB to ENU coordinates (East, North, Up) after recovery using the transformation matrix provided by the manufacturer. The 2 MHz ADCP have a lower particle size detection limit of 12 μm in diameter, and a maximum sensitivity for particles of 242 μm diameter (Haalboom et al., 2021, 2023). The combined
155 optical backscatter sensor for turbidity and fluorescence was programmed to measure every 10 minutes over the one-year

period. The sediment trap (PPS 4/3, Technicap Inc.) with a surface area of 0.05 m² was equipped with twelve bottles for suspended particulate matter collection and with the aperture mounted at 2 m above the bottom. Collection started at 15/08/2018 and lasted until the end of the deployment. Different time intervals of bottle rotation were set to increase sampling resolution during spring and summer months. The bottles rotated every 15 days from mid-August to mid-September 2018, every 30 days from mid-September to mid-November 2018, every 60 days from mid-November to mid-March 2019, then every 30 days from mid-March to mid-May 2019, and every 15 days again from mid-May to mid-July 2019. Prior to deployment, a 4% solution of formalin in brined seawater (40 psu) was added to each bottle.

2.2.2 Water column and benthic sampling

Conductivity-Temperature-Depth (CTD) casts were performed over two cross-shelf transects crossing the LSB and HSB lander sites (Coté et al., 2018; Fig. 1B; Table S1). Two CTD casts were carried out on the continental shelf and three on the continental slope, where the third or middle cast was performed above each benthic lander deployment. The CTD-Rosette water column profiling and sampling package was equipped with a Seabird SBE 911*plus* system, which contained sensors to measure temperature (Seabird SBE 3plus), conductivity (Seabird SBE 4), pressure (Paroscientific Digiquartz®), dissolved oxygen (Seabird SBE 43), fluorescence (Seapoint), and a rosette water sampler with 12 Niskin bottles (12L each). CTD data were processed and “cleaned” with the *Sea-Bird SBE Data Processing* software (Guillot, 2018). Water samples were taken from Niskin bottles at five depths (5 m, 50 m, mid-water, 100 m above bottom, 10 m above bottom) for the determination of nutrients (NH₄⁺, NO₂⁻ + NO₃⁻, PO₄³⁻, SiO₂), and suspended particulate matter (SPM).

Benthic macrofauna samples for stable isotope analysis were collected at the two lander locations using a rock dredge on retrieval of the benthic landers (Coté et al., 2019; Table S3). A description of the species found at the two locations can be found in Coté et al. (2019). The rock dredge (7 mm mesh size) was deployed in “drift” mode at HSB, with a maximum speed of two knots (~4 km h⁻¹) for 10-20 minutes, and “tow” mode at LSB, with the ship moving at one knot for 10 minutes. During CCGS Amundsen cruise 2019 leg1B, it was the first time that a rock dredge was operated on this research vessel, and therefore different operational modes of deployment were tested. At the LSB lander station, the rock dredge collected lots of soft sediment, and therefore “drift” mode was used. On deck, the dredge was rinsed, and the catch was subsampled and deposited in fish totes (64 L). The remaining material was sieved through a 2 mm mesh for analysis of invertebrates and fishes. The total catch was photographed and preserved for species identification and quantification. Samples for stable isotopes were frozen (-20 °C) for further analysis at the Netherlands Institute for Sea Research (NIOZ).

2.2.3 Regional oceanography, sea-ice cover, and bottom temperature/salinity profiles

To explore the regional oceanography on the northern Labrador Shelf and upper slope, vertical Argo float profiles collected within the water depth range 330 - 2575 m (Fig. S3) were extracted from the NOAA NODC World Ocean Dataset and profiling Argo float Global Argo Data Repository archives (Kieke and Yashayaev, 2015; Yashayaev and Loder, 2017) using the

approach of Kenchington et al. (2017). We used Argo float profile data ($N = 1472$) collected between 2005 and 2022 to determine the seasonal variability in temperature and salinity along the northwest Labrador shelf break. Specifically, seawater properties of the corresponding water layers to the depth of the benthic landers (LSB = 350 – 450 m, HSB = 550 – 650 m depth) were assessed. We report the mean temperature and salinity values binned per water layer. Argo float profiles below $\sim 59^\circ$ N latitude were considered LSB and above as HSB. Temperature and salinity values were detrended for interannual variability using an 8th degree least-square polynomial fit. Time-average surface currents were derived from trajectories of satellite-tracked surface drifting buoys (drifters) deployed within the NOAA Global Drifter Program during 2000–2020 (Centurioni et al., 2019). The trajectories were obtained from delayed-mode hourly data and real-time variable time-step data (Elipot et al., 2016, 2022). The drifter data were temporally interpolated into 15-min time intervals, binned hourly, and a low-pass filter was used to remove tidal and inertial oscillations. Then, the surface velocities were binned into a $1/3^\circ$ grid. The drifter-derived surface currents reveal well-defined large-scale cyclonic circulation of the Labrador Sea, recirculation gyres, and mesoscale circulation features.

Sea-ice cover above the two benthic landers was extracted from weekly ice charts (Latest Ice conditions, 2022). Slope angle and aspect was estimated for each lander by taking the wider topography into account (Fig. S1; Gille et al., 2004). Along-slope and across-slope bottom velocities are derived from the bottom current direction, slope aspect, and bottom horizontal current speed.

2.3 Laboratory analysis

Water column nutrient concentrations were analysed with a SEAL QuAATro analyser (Bran + Luebbe, Norderstedt, Germany) following standard colorimetric procedures. SPM samples were freeze-dried, weighed, and analysed for organic carbon content and total nitrogen content.

Sediment trap samples were filtered through a 1 mm sieve to remove large particles and swimmers, then split into five subsamples using a McLane WSD-10 rotary splitter, rinsed with demineralized water to remove salts and formalin and subsequently freeze-dried and weighed (Mienis et al., 2012; Newton et al., 1994). Lipids were extracted and analysed following the method of Kiriakoulakis et al. (2004). Briefly, samples were spiked with internal standard ($5\alpha(\text{H})$ -cholestane), extracted by sonication in dichloromethane:methanol (9:1; x3). The solvent was removed and samples were first trans-methylated (Christie, 1982) and then treated with bis-trimethylsilyltrifluoroacetimide: trimethylsilane (99:1; 30-50 μL ; 60 $^\circ\text{C}$; 1 h) prior to analysis by gas chromatography-mass spectrometry (GCMS). GCMS analyses were conducted using a GC Trace 1300 fitted with a split-splitless injector and column DB-5MS (60m x 0.25mm (i.d.), with film thickness 0.1 μm , non-polar stationary phase of 5% phenyl and 95% methyl silicone), using helium as a carrier gas (2 mL min^{-1}). The GC oven was programmed after 1 minute to rise from 60 $^\circ\text{C}$ to 170 $^\circ\text{C}$ at 6 $^\circ\text{C min}^{-1}$, then from 170 $^\circ\text{C}$ to 315 $^\circ\text{C}$ at 2.5 $^\circ\text{C min}^{-1}$ and was then held at 315 $^\circ\text{C}$ for 15 min. The eluent from the GC was transferred directly *via* a transfer line (320 $^\circ\text{C}$) to the electron impact source of a

220 Thermoquest ISQMS single quadrupole mass spectrometer. Typical operating conditions were: ionisation potential 70 eV; source temperature 215°C; trap current 300 μ A. Mass data were collected at a resolution of 600, cycling every second from 50– 600 Daltons and were processed using Xcalibur software.

225 Compounds were identified either by comparison of their mass spectra and relative retention indices with those available in the literature and/or by comparison with authentic standards. Quantitative data were calculated by comparison of peak areas of the internal standard with those of the compounds of interest, using the total ion current (TIC) chromatogram. The relative response factors of the analytes were determined individually for 36 representative fatty acids and sterols using authentic standards. Response factors for analytes where standards were unavailable were assumed to be identical to those of available compounds of the same class.

230

Sponges and other benthic fauna collected using a rock dredge were subsampled on-board the CCGS Amundsen, as parts of the specimens' bodies were used in separate studies and parts for isotopic analysis in this study. In the laboratory, the collected fauna was freeze-dried and homogenized with a pestle mortar/ball mill. Subsamples (*ca.* 10 mg) were transferred into silver cups and acidified by addition of dilute HCL (2%, 5%, and 30%) to remove carbonates. Organic carbon and $\delta^{13}\text{C}$ were analysed on acidified subsamples, and total nitrogen and $\delta^{15}\text{N}$ was determined on non-acidified subsamples using an Electron Analyser coupled to an Isotope Ratio Mass Spectrometer (Thermo flash EA 1112). $\delta^{13}\text{C}$ and $\delta^{15}\text{N}$ isotope values are expressed in parts per thousand (‰) relative to the international standard Vienna Pee Dee Belemnite and atmospheric N_2 for carbon and nitrogen, respectively. Standard deviation of $\delta^{13}\text{C}$ and $\delta^{15}\text{N}$ measurements was 0.15 ‰.

240

2.4 Data analysis

2.4.1 Data processing

The transformation of beam coordinates to ENU coordinates for the ADCP data was carried out in MATLAB (MATLAB, 2010), and other data processing steps used R. The following R packages are used during data analysis: oce, ggplot2, RColorBrewer, cowplot, knitr, reshape2, RNetCDF, readxl, lubridate, xts, ggalt, tibble, dplyr, clifro, mapdata, metR, patchwork, tibbletime, readr, signal, axtsa, terra, and raster (Becker and Brownrigg, 2022; Campitelli, 2021; Grolemond and Wickham, 2011; Kelley and Richards, 2020; Lovelace et al., 2022; Michna and Woods, 2019; Müller and Wickham, 2023; Neuwirth, 2014; Pedersen, 2019; R Core Team, 2019; Ryan and Ulrich, 2024; Seers and Shears, 2015; signal developers, 2014; Stoffer, 2020; Vaughan and Dancho, 2020; Wickham, 2007, 2016; Wickham and Bryan, 2019; Wilke, 2019; Xie, 2020). Statistics are presented as means \pm standard deviations.

2.4.2 Benthic lander analysis

250 Occasionally, pitch and roll data from the ADCP sensor at HSB were shifted for a small period of the deployment, implying the lander was occasionally moving slightly (Fig. S3). Pitch/heading/roll was almost identical before and after these disturbances. Furthermore, the ADCPs correct for the pitch/roll/heading of the respective device when producing the raw beam data. Removing datapoints during disturbance did not change the outcome of any of the analyses, statistical tests, or descriptive statistics and therefore datapoints were retained in the HSB lander time series.

255

Chl-*a* concentration (in $\mu\text{g L}^{-1}$) and turbidity (in Nephelometric Turbidity Unit; NTU) were calculated from ping counts as described in the manual of the manufacturer.

Spectral analyses of lander data based on a Fourier transformation (Bloomfield, 2004) were performed to examine recurring patterns or periodicity in the time-series data (e.g. Shumway et al., 2000; Bloomfield, 2004). Prior to these analyses, time series data were smoothed using modified lowpass Daniell filters (Bloomfield, 2004), to remove periodicities shorter than 3 hours. The magnitude and direction of ADCP-recorded tidal currents were analysed with least-squares harmonic analysis.

260

2.4.3 Critical-slope and comparing barotropic with baroclinic tides

Internal tides are generated by the barotropic tide interacting with sloping bottom topography and can have a profound influence on the thermohaline structure and local mixing processes. Internal tides are found at complex deep-sea topographic features such as continental shelves, ridges, seamounts and canyons (e.g., Cacchione et al., 2002). Internal tide – topography interactions can be classified by the slope parameter α / c (St Laurent and Garrett, 2002; Cacchione et al., 2002). The internal wave slope c is calculated with Eq. 1:

265

$$270 \quad c = \sqrt{\frac{\omega^2 - f^2}{N^2 - \omega^2}} \quad (1)$$

with tidal frequency $\omega = 1.4053\text{e-}4 \text{ rad s}^{-1}$ (representing the dominant M2 tidal component) and local inertial frequency f (s^{-1}). The Brunt-Väisälä frequency N^2 (rad s^{-2}) was calculated as the mean value ($1.4228 * 10^{-5} \text{ rad s}^{-2}$) from all CTD stations and depths below the deep pycnocline at 250 m or from bottom values at shallower profiles. The topographic slope α was calculated from the maximum depth gradients in latitude and longitude based on GEBCO_2023 data (GEBCO Bathymetric Compilation Group, 2023). At critical or near-critical slopes ($\alpha \approx c$), the internal tide is locally amplified and vertical mixing is intensified. At subcritical slopes ($\alpha < c$), internal waves pass the topographic slope without being locally modified. At steeper supercritical slopes ($\alpha > c$), internal waves are reflected into deeper waters. Bottom currents and direction were compared to model derived barotropic tidal currents, retrieved from the Oregon State University (OSU) Tidal Inversion Software (OTIS; Egbert and Erofeeva, 2002).

275

3.1 Seawater properties over the northern Labrador Shelf and upper slope

The CTD casts, performed in July 2018, revealed different seawater properties between the two transects (Fig. 3; Fig. S4). The surface water at the time of survey was relatively warm (2 – 6 °C) and fresh (31.2 to 33.8 psu) showing an offshore increase in temperature and salinity. From the surface to the depth of 20-70 m, depending on the transect and location, temperature
285 decreased to sub-zero or near-zero at the shelf locations, to 3 °C at the slope locations, and then increased again to 2.8 °C at 250 m depth on the shelf and to 4.3°C at 150 m on the slope. A cold intermediate layer was visible at all profiles between 50 – 150 m depth. Salinity increased nearly monotonically with depth up to the pycnocline across all stations. The stations at LSB were more saline overall than those at the matching water depths on the HSB transect. Buoyancy frequency showed peak values at the upper- and lower boundaries of the above described cold intermediate layer at both transects (Fig. S4F).

290

The oxygen concentration was highest in the surface waters (0 – 50 m) on the shelf and decreased with depth at all CTD stations (Fig. 4A). Although oxygen concentrations were still generally high, the bottom oxygen concentrations at the lander stations were, for both transects, relatively depleted compared to the deep water CTD transects at similar depths. Concentrations of nitrate, phosphate, and silicate were lowest above the thermocline and increased with depth, while
295 ammonium and nitrite were higher near the surface than at depth (Fig. 4B & C, Fig. S5). The HSB station exhibited relatively high nitrate, phosphate, and silicate concentrations at 10 and 100 metres above bottom compared to similar depths at shelf and deep stations (Fig. 4B & C, Fig. S5). This increased nutrient concentration in the bottom waters was also apparent for silicate at the LSB station (Fig. 4C), but not for nitrate (Fig. 4B). Chl-*a* profiles showed a deep chlorophyll maximum along both transects at 50 m (Fig. 4C), and near-zero concentrations in the bottom waters (Fig. S4D). Particulate organic carbon (POC)
300 concentrations were highest in the surface waters (8 – 38 $\mu\text{mol POC L}^{-1}$) and on the shelf (Fig. S6:). POC concentrations decreased with depth, and concentrations 10 m above bottom were 1.48 $\mu\text{mol POC L}^{-1}$ at HSB, and 5.95 $\mu\text{mol POC L}^{-1}$ at LSB.

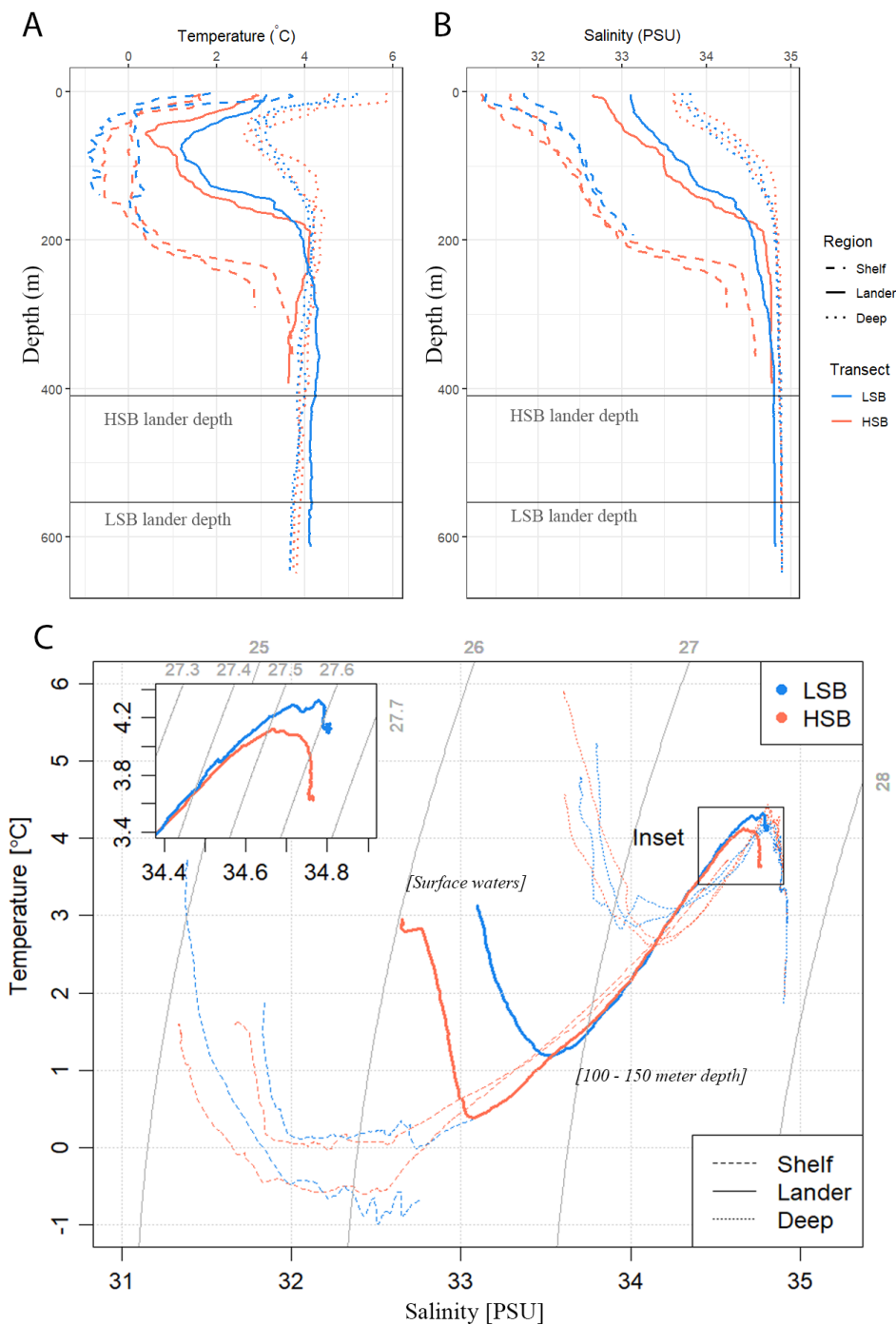
Surface water above the benthic lander locations was partly ice-covered from December to June, but both sites were located at the sea-ice border in the study area and ice cover was highly variable (Fig. S11). Only during January ice-coverage was
305 above 70% at both sites. Both locations showed a short ice-free period in February and March. During the spring bloom, between the end of March and early May, sea-ice coverage tended to be higher at HSB than at LSB (Fig. S11D).

3.2 Regional oceanography and seasonal temperature patterns

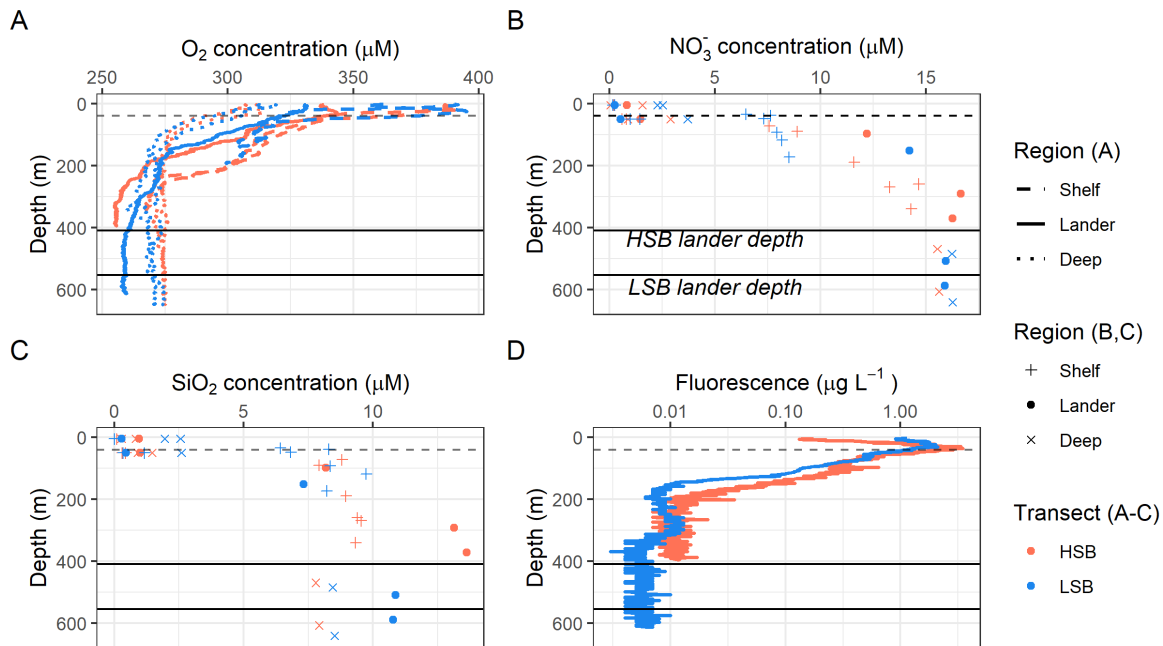
Surface buoy drifter data showed that the HSB lander was located in an area where three (surface) currents converge (Fig. 5A).
310 Strong surface currents ($>0.24 \text{ m s}^{-1}$ on average) carry water from the Hudson strait towards the Labrador shelf break, where

this current meets two others that, respectively, flowed toward the HSB site from the north and northeast. On convergence, the currents followed the bathymetry of the Labrador shelf break or upper slope southwardly.

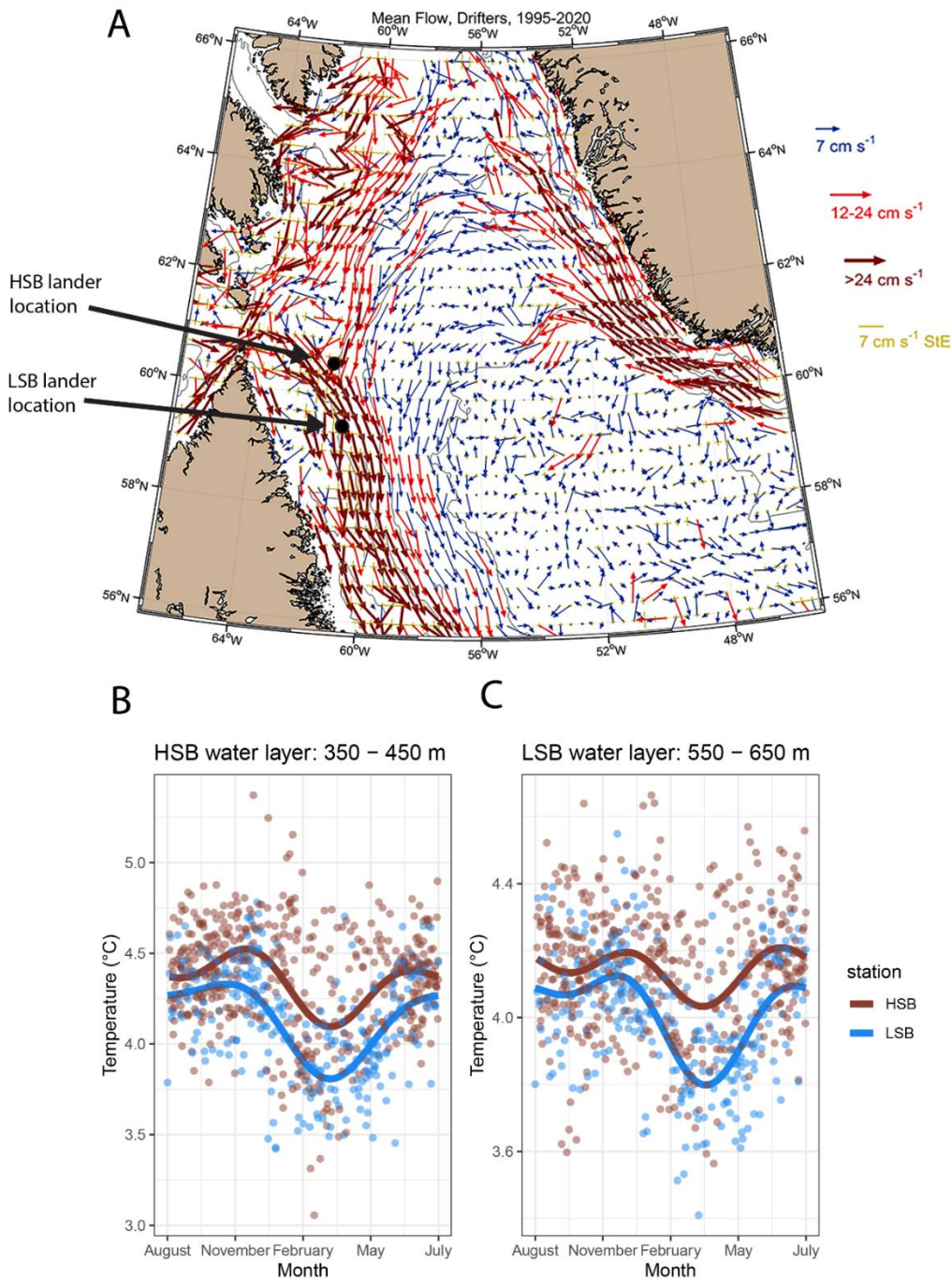
315 The seawater in the region of HSB was warmer and less saline than around LSB for both depth ranges within which the landers were deployed (Fig. 5B & C; Fig. S7). Bottom water temperature shows a steeper decrease in February at LSB compared to HSB (Fig. 5C). Temperature and salinity show higher scatter at HSB than LSB throughout the season, but variability in temperature is highest at HSB in February/March (Fig. 5B & C; Fig. S7).



320 **Figure 3: Hydrographic conditions in the study area: (A) temperature, (B) salinity and (C) temperature – salinity (TS) plots for the two transects. LSB = low-sponge-biomass, HSB = high-sponge-biomass. Depths of landers are indicated by the horizontal grey lines in A and B. Temperature and salinity profiles in A and B only show top 600 m, while TS plots include the entire water column. The thin grey lines in subplot C resemble isopycnals.**



325 **Figure 4: Oxygen (A), nitrate (B), silicate (C) concentration profiles for the two transects, and D) fluorescence profiles for the two CTD casts above the two lander locations. HSB = high-sponge-biomass site, LSB = low-sponge-biomass site. Black lines indicate lander depths, dashed line indicates thermocline.**



330 **Figure 5:** A) general surface circulation pattern in the Labrador Sea based on drifter buoy data spanning from 1995 - 2020. Arrows indicate mean direction, colours and length of arrow present the strength of the mean flow, the yellow arrows present the standard error of the flow over 1995 – 2020. The lander locations are indicated by the coloured dots. B & C) seasonal temperature, from Argo float profiles, of the water layer in which HSB/LSB lander was located. Dots represent individual water-layer-binned temperature measurements vs. date of the year. The lines are a smoothed fit that show the seasonal pattern.

3.3 Year-long near-bottom measurements

335 3.3.1 Near-bottom current velocities

In general, bottom current speeds were higher at the HSB compared to the LSB station (Table 1; Fig. 7). General current direction was south-easterly at HSB and south-south-westerly at LSB (Fig. 6). Vertical velocity (w) was on average upward and comparable between HSB and LSB, but the range in vertical velocity was higher at HSB (-0.35 to 0.32 m s^{-1}) compared to LSB (-0.11 to 0.21 m s^{-1} ; Fig. 7C). Bottom horizontal currents were twice as high at HSB than at the LSB (Table 1), and peak bottom horizontal current speeds were 0.75 m s^{-1} (HSB) and 0.65 m s^{-1} (LSB), with the third quantile at 0.33 m s^{-1} (HSB) and 0.18 m s^{-1} (LSB).

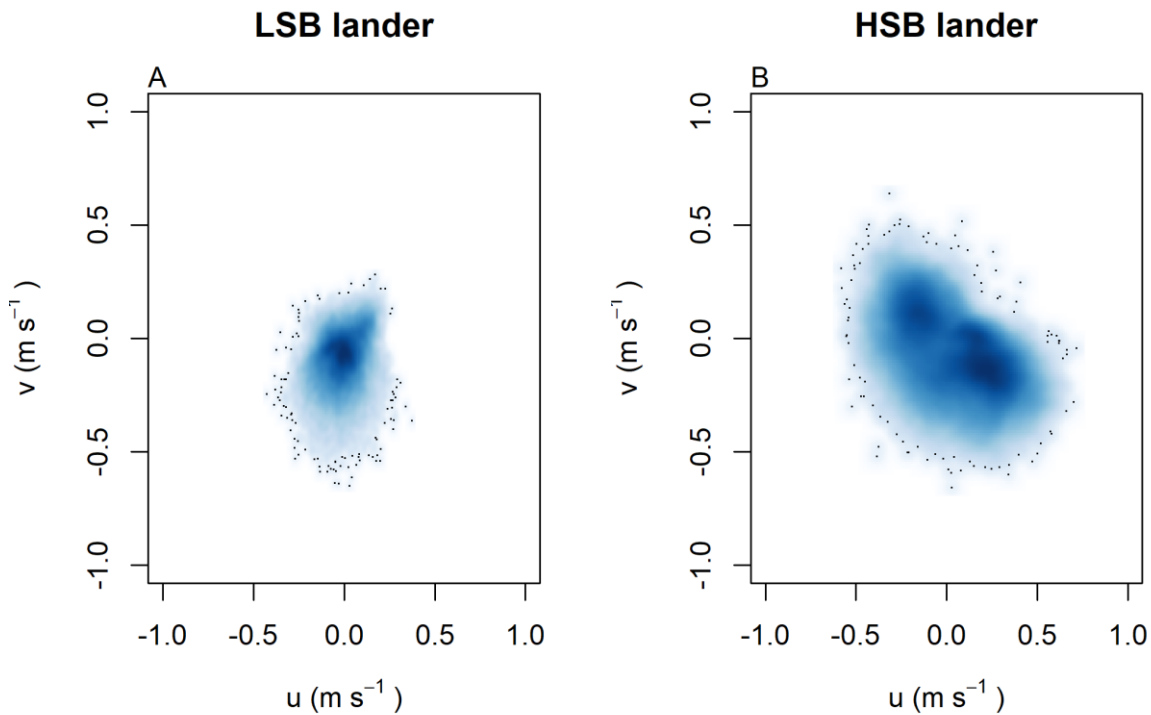


Figure 6: horizontal current velocities at A) LSB lander and B) HSB lander.

3.3.2 Near-bottom environmental conditions

345 Bottom temperature was slightly warmer at HSB compared to LSB and increased at both sites ($0.2 - 0.3$ $^{\circ}\text{C}$) during December and January (Fig. 9). The benthic lander temperature aligned well with the seasonal temperature pattern retrieved by Argo float profiles (Fig. 5 B & C). Turbidity measured by ABS was similar for the two stations (Table 1; Fig. 9 B) and showed higher values in winter months. Chl- a remained low from October to February/March values started to increase for both landers (Fig.

9 C). Bottom chl-*a* concentrations started to increase after short ice-free period mid-February and mid-March Fig. 9C; Fig. 350 S11D). The HSB station showed highest chl-*a* concentrations from mid-March to the end of May, while at the LSB station increased concentrations were observed from mid-March to early May.

Turbidity measured by OBS was elevated at HSB from February to April, and at LSB from December to January. The higher variability in chl-*a* and turbidity at the LSB site over the year (Table 1) was caused by several peaks in chl-*a* and turbidity that were an order of magnitude higher than average values (Fig. S8).

355 During several periods in the year-long time-series, turbidity measured by the ABS increased at the turning of the tide and at high south-easterly current velocities at HSB (see e.g. Fig. 10F). Strong along slope (southerly) bottom currents increased ABS turbidity and OBS turbidity at LSB (Fig. 10F). Cross-and along slope water transport influenced bottom temperature. At the HSB lander, for example, in the first week of September, temperature decreased when the current was directed northwest and increased when the current was directed southeast (Fig. 10 A-E).

360 **Table 1: Benthic lander mean and standard deviations over the year-long deployment period. Values are given as mean \pm standard deviation. HSB = high-sponge-biomass lander, LSB = low-sponge-biomass lander. ABS = acoustic backscatter signal. OBS = optical backscatter signal**

Variable	HSB	LSB
<i>u</i> (eastward velocity; m s ⁻¹)	0.05 \pm 0.22	-0.01 \pm 0.09
<i>v</i> (northward velocity; m s ⁻¹)	-0.07 \pm 0.16	-0.09 \pm 0.11
<i>w</i> (vertical velocity; m s ⁻¹)	0.03 \pm 0.05	0.02 \pm 0.03
Bottom current speed (m s ⁻¹)	0.26 \pm 0.14	0.14 \pm 0.08
Temperature (°C)	3.70 \pm 0.17	3.58 \pm 0.17
Daily temperature variability ($\Delta^\circ\text{C d}^{-1}$)	0.25 \pm 0.16	0.17 \pm 0.1
Turbidity by ABS (counts)	98.1 \pm 9.8	96.6 \pm 11.0
Chl- <i>a</i> concentration ($\mu\text{g L}^{-1}$)	0.11 \pm 0.03	0.08 \pm 0.10
Turbidity by OBS (NTU)	0.20 \pm 0.10	0.21 \pm 0.27
Across slope velocity (m s ⁻¹)	0.01 \pm 0.13	-0.01 \pm 0.01
Along slope velocity (m s ⁻¹)	-0.08 \pm 0.23	-0.09 \pm 0.11

3.3.3 Tidal analysis of bottom currents and environmental conditions

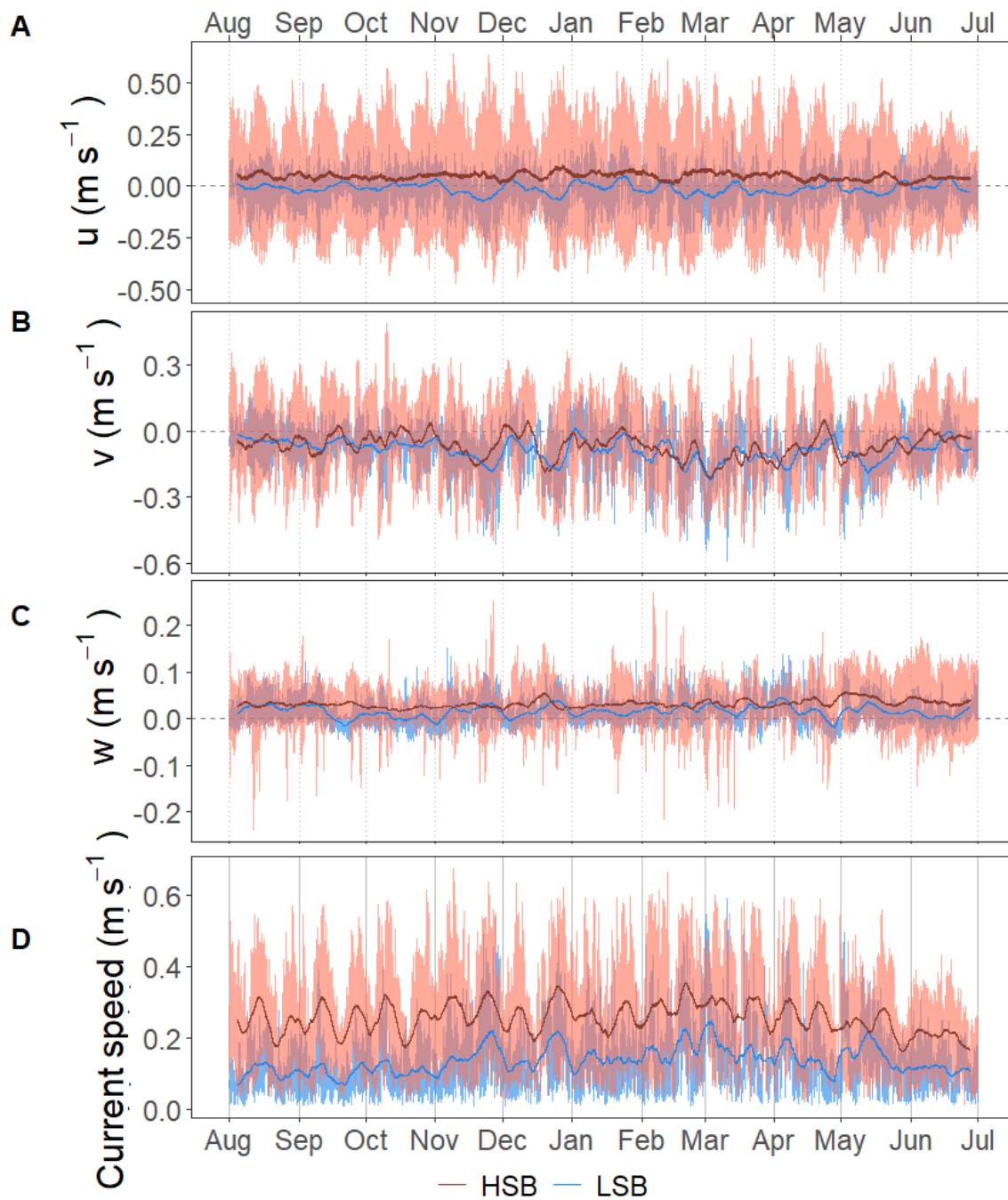
365 Bottom current speeds showed semi-diurnal and spring-neap tidal patterns, with a peak every fortnight for both sites (Fig. 7 C; Fig. 8 B; Fig. 10). The major axes of the semidiurnal tidal ellipses were directed in a northwest-southeast direction at HSB and a north-south direction at LSB (Fig. 7D). The tidal analysis presented in Table 2 and Fig. 8 shows notable differences in tidal characteristics between the LSB and HSB lander locations. While semidiurnal tidal harmonics predominate at both locations, the semi-major axis at the HSB site is approximately four times larger than the corresponding value at the LSB site. 370 Moreover, there is a significant discrepancy between the modelled and observed main semidiurnal tidal harmonics (M2) at the HSB site, particularly in terms of magnitude and tidal ellipse eccentricity. This indicates that the dominant barotropic

semidiurnal tide (M2) is altered at the HSB site, leading to strongly rectified near-bottom baroclinic tidal currents. There are no substantial differences between the modelled (barotropic) and observed S2 tidal currents, except for the tidal ellipse eccentricity at the LB site, likely due to the depth difference between the model and observations at this location. Furthermore, spectral density for the HSB bottom current components also peaked at shorter frequencies (3-6 h) and at the fourteen-day spring-neap tide (Fig. 8B). In addition, a superimposed seasonal pattern can be seen at both sites, where the bottom current speed gradually increased from July 2018 to March 2019 and decreased again from March 2019 to July 2019.

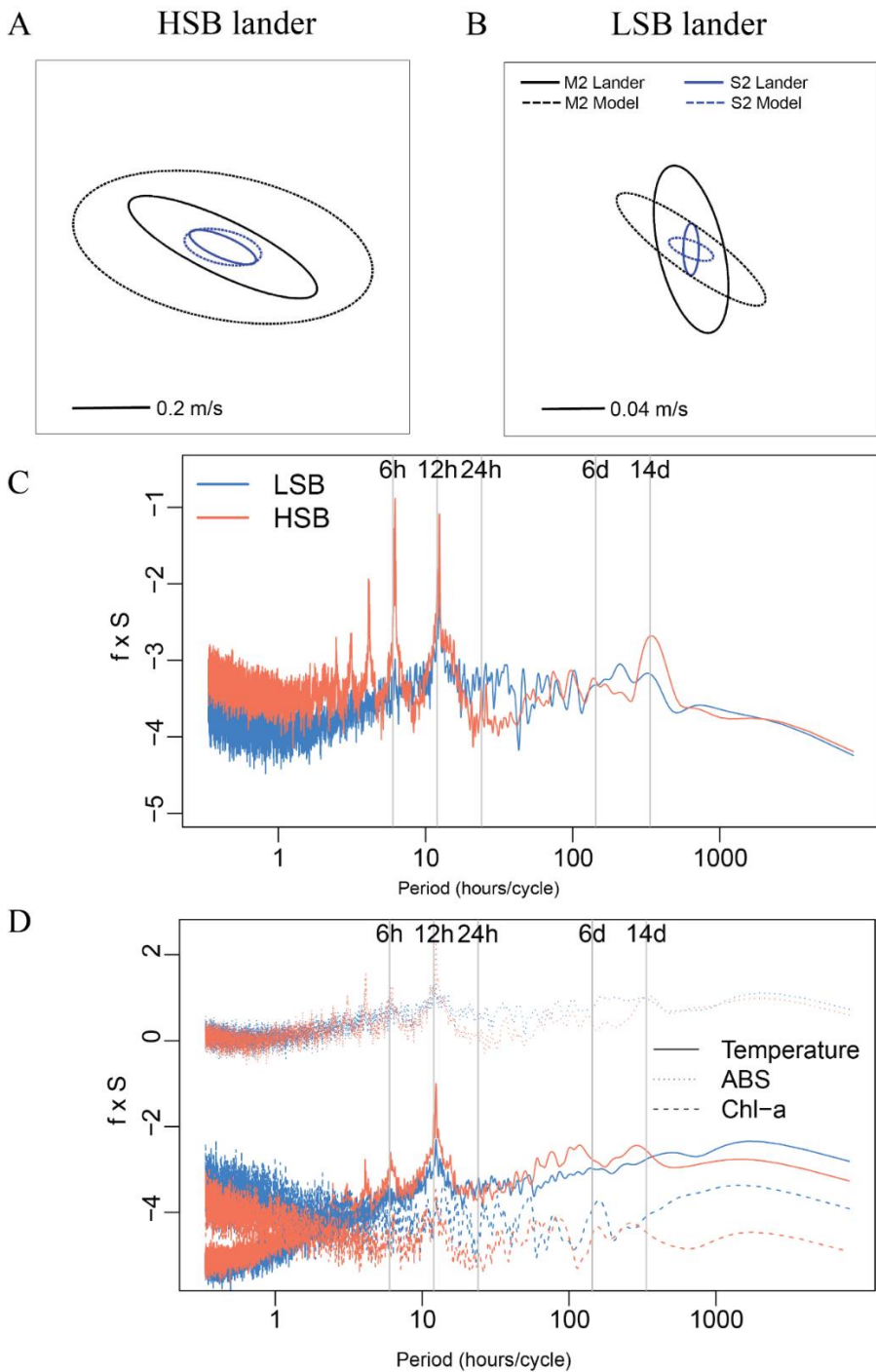
Table 2: Tidal analysis of velocity time series from the HSB and LSB lander sites based on ADCP measurements and OTIS tidal model analysis. a_{maj} and a_{min} are the semi-major and semi-minor axes of the tidal ellipse and ϵ is the eccentricity (a_{min}/a_{maj}). OTIS model data represent the barotropic tidal signal, whereas ADCP data show the near-bottom tidal characteristics.

LSB – lander data	a_{maj} (cm s ⁻¹)	a_{min} (cm s ⁻¹)	ϵ (a_{min}/a_{maj})	Water depth (m)
M2	5.73	2.17	0.38	558
S2	1.74	0.51	0.30	
K1	0.65	0.05	0.08	
O1	0.10	0.03	0.25	
HSB – lander data				
M2	27.77	7.26	0.26	410
S2	9.61	2.88	0.30	
K1	0.88	0.44	0.51	
O1	0.36	0.21	0.58	
LSB – OTIS tidal model				
M2	6.08	1.48	0.24	629
S2	1.58	0.57	0.36	
K1	0.49	0.06	0.11	
O1	0.18	0.01	0.04	
HSB – OTIS tidal model				
M2	40.67	19.23	0.47	425
S2	10.45	4.47	0.43	
K1	1.35	0.53	0.39	
O1	0.80	0.38	0.48	

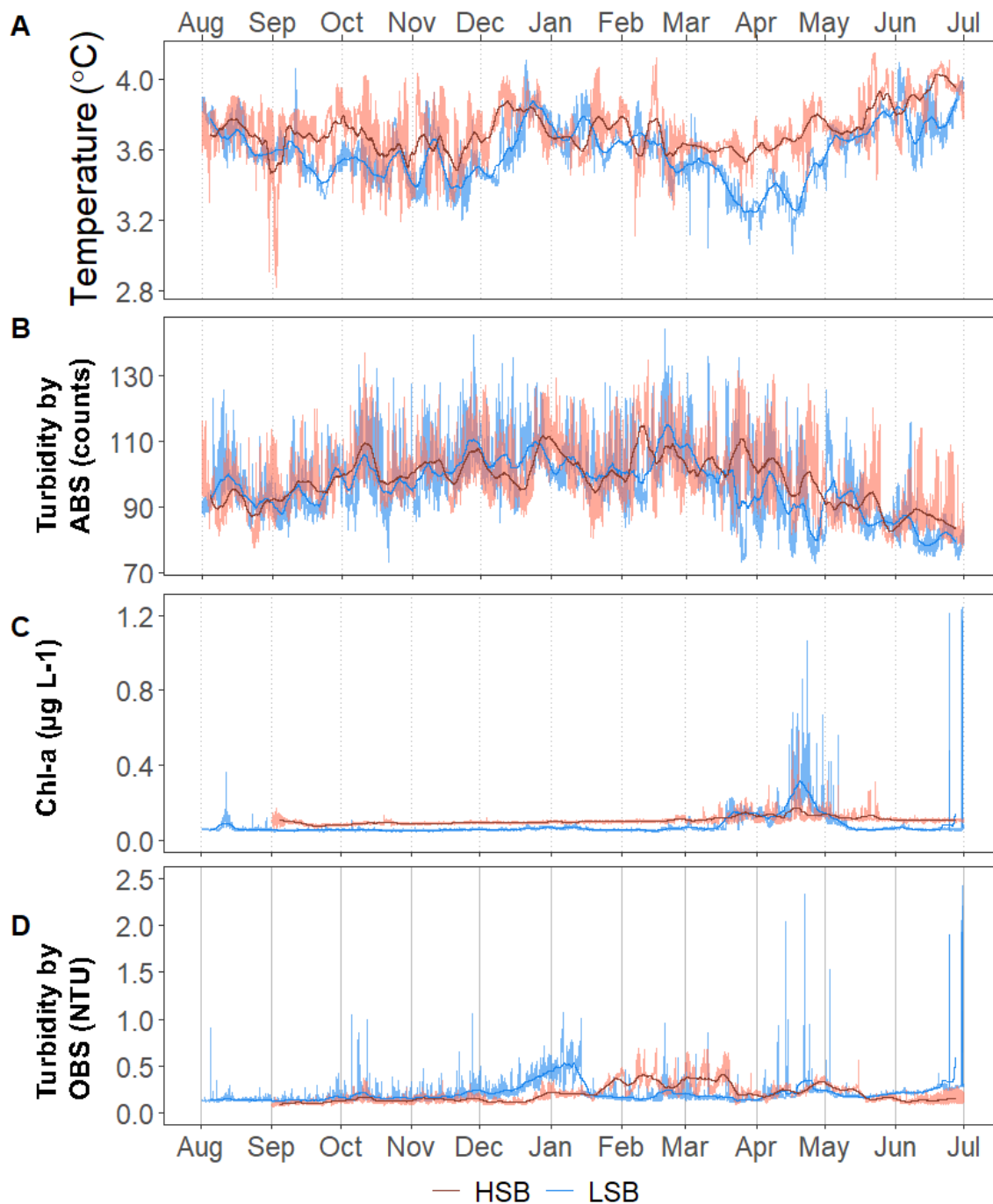
Temperature, chl-*a*, turbidity measured by ABS and OBS, all showed a reoccurring tidal peak, with higher peaks in spectral density for the semidiurnal periodicity at HSB than at LSB (Fig. 8C). Daily temperature fluctuations were higher at HSB than
385 at LSB. During the spring bloom, bottom chl-*a* concentration increased during strong south-easterly current velocities at HSB (Fig. S10) and showed a periodic reoccurring peak (Fig. S11A).



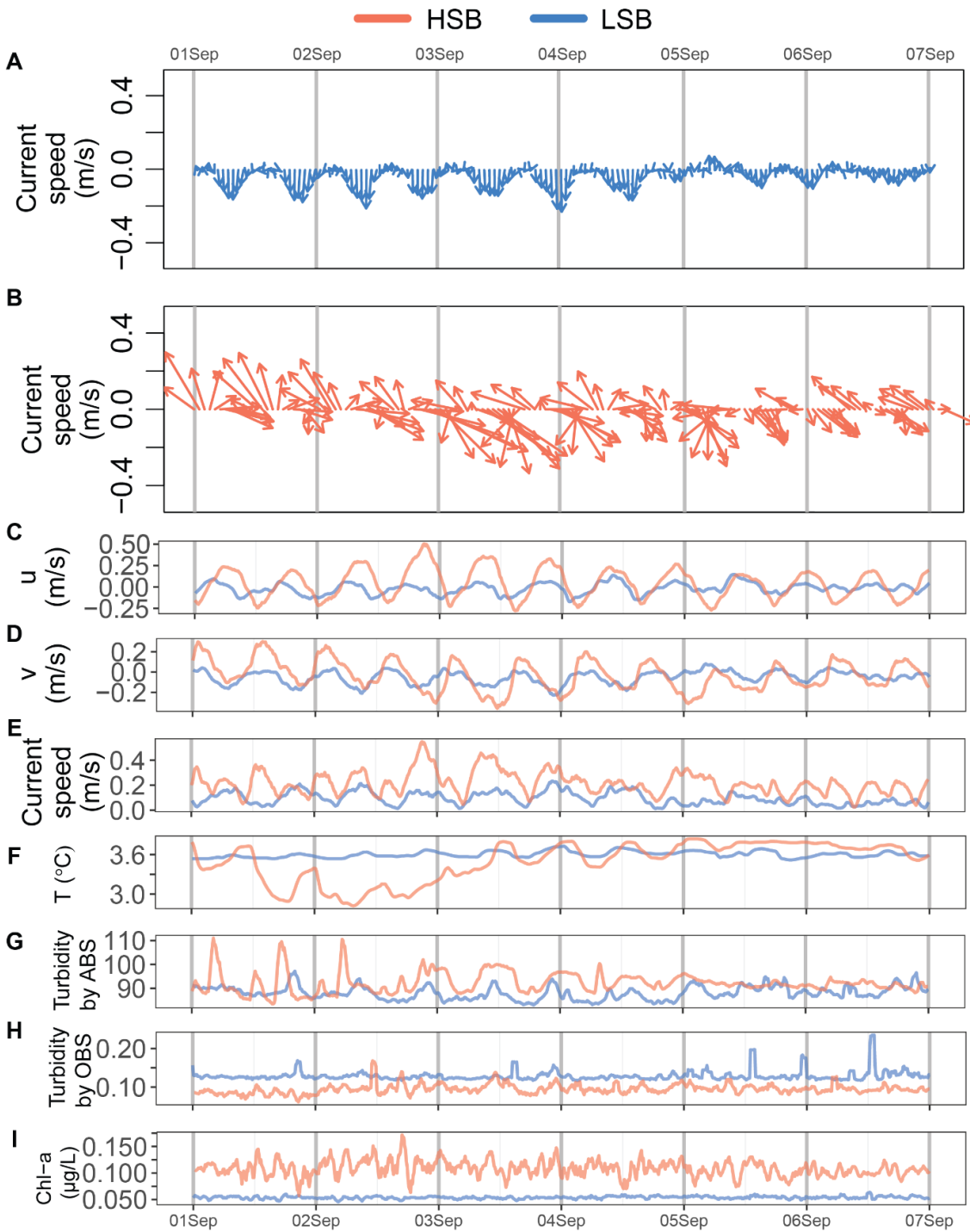
390 **Figure 7: Time series of the flow velocities with eastward u velocity (A), northward v velocity (B), vertical w velocity (C), and bottom current speed (D). Plots show the hourly averaged data as transparent lines and the seven-day rolling means as solid lines.**



395 **Figure 8: A & B) Tidal current ellipses at the HSB and LSB lander sites for the two dominant semidiurnal tidal harmonics M2 (black lines) and S2 (blue lines) derived from the unfiltered ADCP velocities (solid lines) and the OTIS inverse tidal model (dashed lines) respectively. Variance preserving spectra for C) bottom current speed, D) temperature, turbidity by acoustic backscatter signal (ABS), and chl-a.**



400 **Figure 9:** Time series for temperature in °C (A), Turbidity by acoustic backscatter (ABS; in counts) (B), Chl-a concentration in µg L⁻¹ (C), and turbidity by optical backscatter (OBS) in NTU (D). Plots C and D are limited on the y-axis to 1.25 µg L⁻¹ and 2.5 NTU, respectively, for clarity. Chl-a and turbidity by OBS data without the Y-axis cut-offs are plotted in Fig. S10.

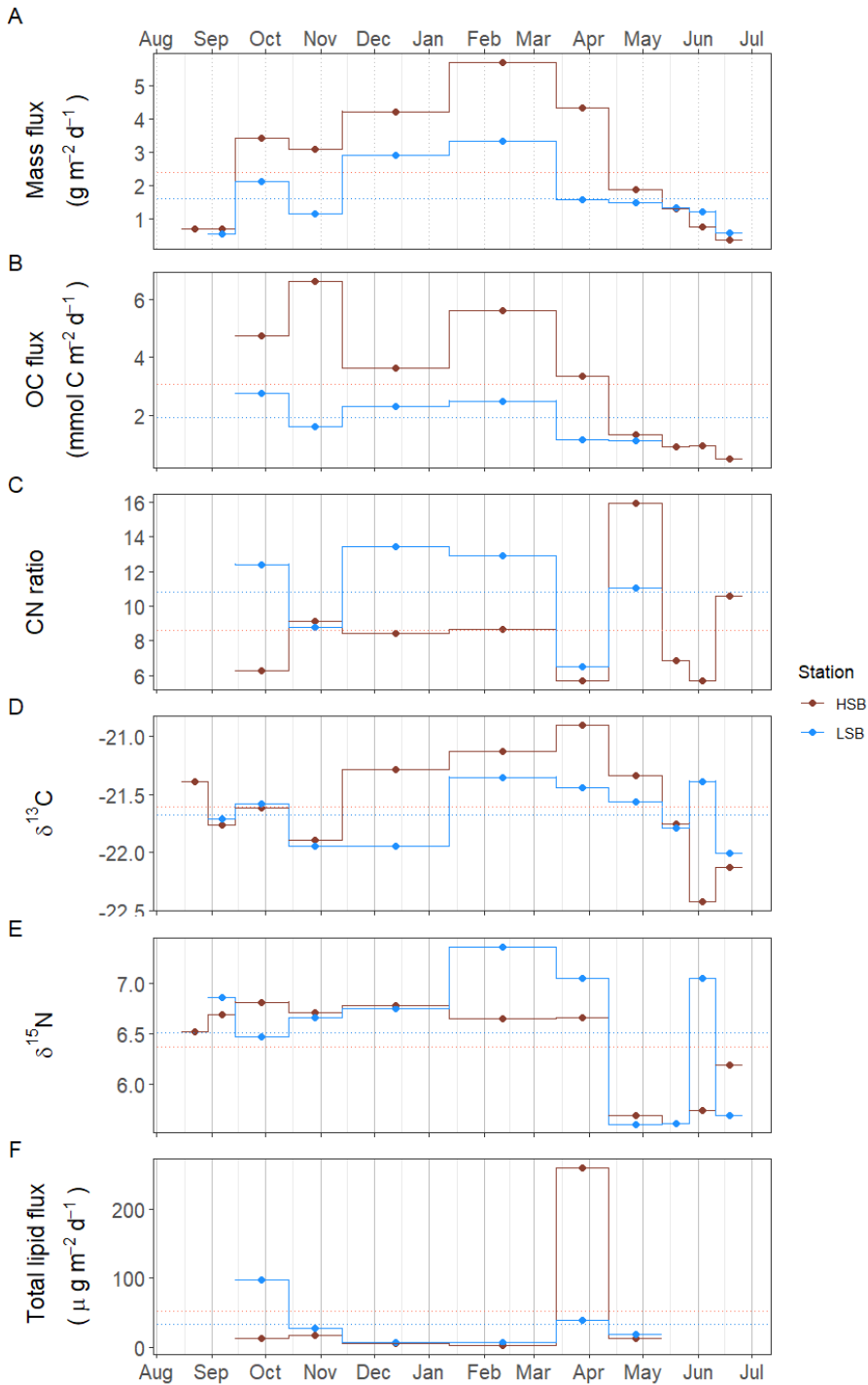


405

Figure 10: Expanded detail for the first week of September for the current direction at LSB (A), current direction at HSB (B), eastward velocity (C), northward velocity v (D), bottom current speed (E), temperature (F), turbidity by acoustic backscatter (ABS; G), turbidity (H), and chl-a concentration (I).

3.4 Mass deposition and organic carbon fluxes

The average mass fluxes were higher at HSB ($2.46 \pm 1.76 \text{ g m}^{-2} \text{ day}^{-1}$) than at LSB ($1.43 \pm 0.93 \text{ g m}^{-2} \text{ day}^{-1}$), with highest fluxes in winter (October to April) at both sites, which corresponds well with the superimposed seasonal patterns seen in ABS turbidity and bottom current speed. Average POC fluxes were higher at HSB ($3.07 \pm 1.91 \text{ mmol C m}^{-2} \text{ d}^{-1}$) than at LSB ($1.91 \pm 0.71 \text{ mmol C m}^{-2} \text{ d}^{-1}$). Organic carbon content at HSB was highest in autumn/summer months (~2 %) and highest at LSB in autumn (2-4%; data not shown). Average C:N ratios were lower at HSB (8.6 ± 3.2) than at LSB (10.8 ± 2.7) and were higher in winter and also in May 2018 (Fig. 11C). The $\delta^{13}\text{C}$ ratios of trapped material were higher in winter at HSB compared to LSB, and were higher in summer at LSB than at HSB (Fig. 11D). The $\delta^{15}\text{N}$ of trapped material was comparable between sites, although slightly higher at LSB. Winter $\delta^{15}\text{N}$ values were highest compared to the rest of the year for both landers (Fig. 11E). The lipid flux was slightly higher at LSB, with low values in winter and peak values during the spring bloom (Fig. 11F). Unsaturated alcohols comprised the largest fraction of lipids at LSB, especially in autumn and winter (Fig. S12B). Peak lipid flux in April consisted of 25% polyunsaturated fatty acids (PUFAs) at HSB (Fig. S12C). Sterols made up the largest fraction of total lipids at HSB and LSB in May (Fig. S12D). The sterol fraction was lower in spring at both sites. Swimmers were found in the sediment trap bottles, especially in the autumn months at LSB. These consisted mostly of copepods (e.g., *Calanus* sp.), mysids (e.g., *Boreomysis* sp.), amphipods (e.g., Eusiridae) and chaetognaths (i.e., arrow worms). Numbers of trapped swimmers were lowest during winter at both sites. In addition, several large sponge spicules were found in the bottles at HSB, but not at LSB.



425

Figure 11: Sediment trap content from the two benthic landers. HSB = high-sponge-biomass lander, LSB = low-sponge-biomass lander. A) mass flux in $\text{g m}^{-2} \text{d}^{-1}$, B) organic carbon flux in $\text{mmol C m}^{-2} \text{d}^{-1}$, C) molar C:N ratio of trapped material, D) $\delta^{13}\text{C}$ of trapped material, E) $\delta^{15}\text{N}$ of trapped material, F) total lipid flux in $\mu\text{g m}^{-2} \text{d}^{-1}$.

3.5 $\delta^{13}\text{C}$ and $\delta^{15}\text{N}$ isotopic ratios of benthic fauna and trapped material

430 The massive sponge *Geodia* spp. sampled at HSB showed a distinct isotopic signature compared to the other benthic organisms, with a relatively enriched $\delta^{13}\text{C}$ (-18.55 ± 0.17 ‰) and a low $\delta^{15}\text{N}$ (8.24 ± 0.16 ‰; Fig. 12). The gorgonian coral *Primnoa resedaeformis* had $\delta^{13}\text{C}$ of -21.19 ± 0.59 ‰ and $\delta^{15}\text{N}$ of 10.54 ± 0.33 ‰. Compared to *P. resedaeformis*, Decapoda sp. showed slightly enriched $\delta^{13}\text{C}$ (-20.48 ± 0.31 ‰), and $\delta^{15}\text{N}$ (11.97 ± 0.43 ‰) values. The glass sponge *Asconema* sp., sampled at HSB, also had relatively enriched isotopic values ($\delta^{13}\text{C}$: -20.27 ± 0.36 ‰, and $\delta^{15}\text{N}$: 12.57 ± 0.31 ‰) while the sponge *Mycale* sp.,
435 sampled at LSB, had a high $\delta^{15}\text{N}$ isotopic ratio (13.05 ± 0.41 ‰), and a $\delta^{13}\text{C}$ ratio of -19.47 ± 0.06 ‰. Sediment trap samples had the lowest $\delta^{15}\text{N}$ and $\delta^{13}\text{C}$ isotopic ratios, with only small differences between HSB and LSB (Fig. 11 D & E; Fig. 12).

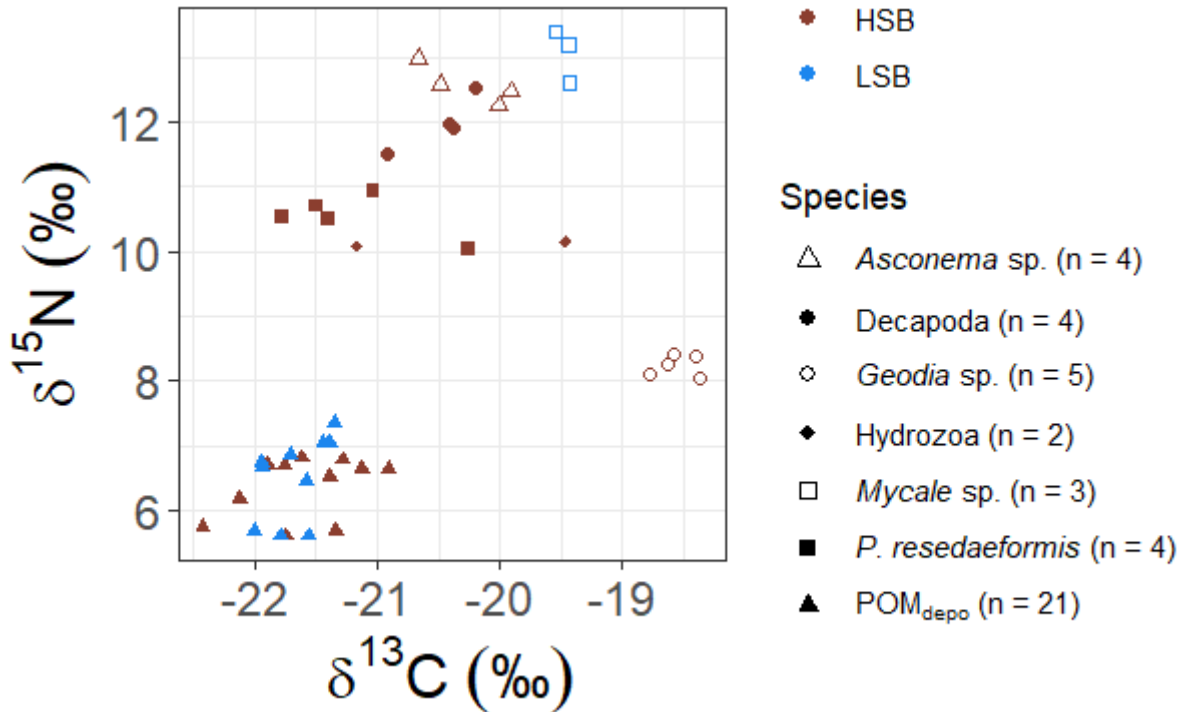


Figure 12: Carbon and nitrogen stable isotopes plots of megafauna and sediment trap samples. HSB = high-sponge-biomass, LSB = low-sponge-biomass.

440

4 Discussion

Hydrodynamic- and environmental conditions were compared at two contrasting high- and low-sponge-biomass sites along the northern Labrador shelf break. The aim was to compare differences between the two sites in terms of (i) seawater properties and regional hydrography (section 4.1, 4.2), (ii) bottom currents and environmental conditions, including seasonal variations
445 over the course of a year (section 4.3, 4.4), and (iii) benthic-pelagic coupling, organic matter supply and isotopic signatures of benthic macrofauna (sections 4.6, 4.6, and 4.7).

4.1 Regional oceanography on the northern Labrador Shelf and Slope

The northern Labrador Shelf and Labrador Slope are known to be subject to strong tidal forcing which causes vertical mixing, high bottom current speeds (Drinkwater and Jones, 1987; Griffiths et al., 1981), and reduced stratification compared to the
450 more northerly Baffin Island Shelf (Lazier 1982; Sutcliffe et al. 1983; Drinkwater and Harding 2001). The results of our drifter analysis confirm that around the HSB area three currents converge: the Hudson Strait Outflow, the Baffin Intermediate Current, and the West Greenland Current (Fig. 5A; Smith et al., 1937; Yashayaev, 2007; Straneo and Saucier, 2008; Curry et al., 2011, 2014). These three currents transport, respectively, Hudson Strait Outflow Water, Arctic Water and/or Baffin Bay (intermediate) Water, and Irminger Water towards the northern Labrador Shelf and upper slope. Our CTD transects show the
455 characteristics of these water masses, and are similar to earlier observations (Drinkwater and Harding, 2001; Fissel and Lemon, 1991; Petrie et al., 1988). The warmer and saltier water at HSB ($\Theta \sim 4.5$ °C and $S \sim 34.9$) compared to LSB is likely caused by Irminger Water (Fig. 5 B & C), which follows the Labrador slope in cyclonic direction beneath the cold water of the West Greenland Current and above the upper slope (Lazier et al., 2002). Our findings concur with previous work which showed that Irminger Water is gradually cooled while moving southward by mixing with the Baffin Island Current (Cuny et al., 2002).
460 However, the Argo float temperature profiles indicate that the area around HSB might play an important role in transforming Irminger Water. For example, the 350-450 m depth layer in the HSB area regularly showed presence of Irminger Water (>4.5 °C), while it was only sporadically measured at LSB (Fig. 5B). Irminger Water might therefore be cooled and freshened in the area around HSB due to convergence and consequently mixing occurs with the Hudson Outflow and Baffin Island Current. Our results support earlier findings that identified a connection between the Hudson Strait outflow strength and the southern
465 Labrador Shelf water based on salinity measurements (Myers et al., 1990; Sutcliffe et al., 1983).

4.2 Increased bottom nutrient concentrations

Both the LSB and HSB lander sites show higher nutrient concentrations in the bottom water compared with the other shelf/deep CTD stations, and this difference was more pronounced at the HSB lander location (Fig. 4). Here we discuss two possible explanations for this observation: large scale advection of nutrient-rich water from Baffin Bay and sediment efflux of silicic
470 acid. Intermediate water flows from Baffin Bay via the Davis Strait southward along the continental slope (Curry et al., 2014). This water mass, referred to as Baffin Bay Water (BBW), contains high nutrient concentrations (e.g., 41.6 ± 25.5 μM $\text{Si}(\text{OH})_4$,

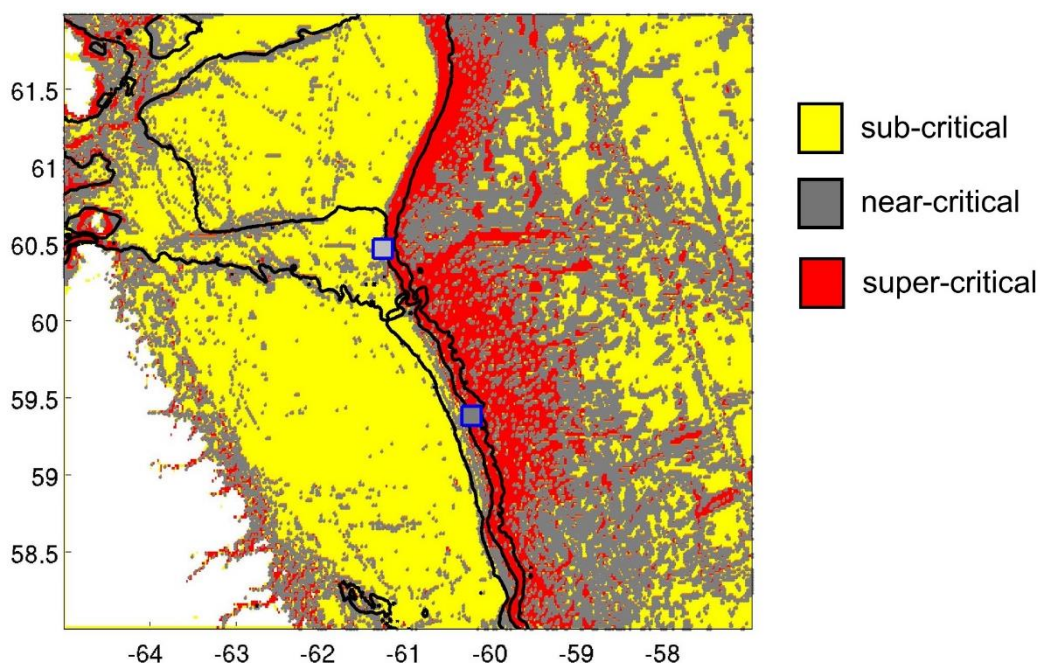
18.5 ± 2.6 μM NO₃⁻; Sherwood et al., 2021) due to *in situ* remineralization of organic matter to deep water circulating in the Baffin Bay basin (Jones et al., 1984; Lehmann et al., 2019; Tremblay et al., 2002). Furthermore, BBW shows relatively high concentrations of silicate and phosphate compared to nitrate, due to denitrification at depth in Baffin Bay (Lehmann et al., 2019; Sherwood et al., 2021). Secondly, high efflux of silicic acid (nutrients) from the sediment could enhance bottom water silicate (nutrient) concentrations. Research on glass-sponge grounds on the Scotian shelf has shown that the biogenic silica efflux from sediments lead to higher bottom silicate concentrations (Maldonado et al., 2020b). This would also be possible for our study area. Given that the silicate concentration was elevated by ~2-3 μM up to 100 meters above the bottom (Fig. 4), assuming that the length of the sponge ground was ~120 km (Fig. 1), and thereby estimating the retention time of a water parcel on the sponge grounds is about 33 days (length sponge ground divided by residual current speed), this would mean that, under the assumption that the bottom 100m is well mixed, a sediment efflux of 6 – 9 mmol Si m⁻² d⁻¹ would be required. While this would be a substantial sediment efflux, silicate effluxes of 2.4 mmol Si m⁻² d⁻¹ have been measured on the Scotian Shelf (Andrews and Hargrave, 1984; Maldonado et al., 2020b), and of up to 14.1 mmol Si m⁻² d⁻¹ in the Laurentian Channel (East Canada; similar depth and temperature; Miatta and Snelgrove, 2021). Nonetheless, the higher silicate concentrations at HSB lander than at LSB lander imply that the source is located closer to HSB. The fact that phosphate was also enhanced in bottom waters at HSB, suggests that advection of nutrient-rich water from upstream is the more probable explanation. However, further work on bottom silicate concentrations in relation to sponge grounds in this area is needed to unravel the source of this excess silicate and investigate if and how sponge grounds benefit from this.

The elevated nutrient concentrations could be beneficial for benthic organisms, specifically, deep-sea sponges, which require silicic acid for spicule formation and skeletal growth (López-Acosta et al., 2016; Maldonado et al., 2011, 2020a; Whitney et al., 2005). Published kinetic uptake curves, describing silicic acid uptake rate *versus* concentration, suggests the concentration at the HSB lander (13.6 μM) compared to LSB shelf (9.3 μM) lead to a higher silicic acid uptake rates at the HSB site of 39% for *Axinella* spp. and 40% for *V. pourtalesii* (Maldonado et al., 2011, 2020a). Furthermore, elevated silicic acid concentrations on a spatial scale of kilometres are thought to allow the persistence of sponge grounds and build-up of (glass) sponge biomass over long timescales (Maldonado et al., 2020b; Whitney et al., 2005).

4.3 Tidal dynamics and bottom current speed

This study, to our knowledge, is the first to report year-long hydrodynamic- and environmental conditions measured simultaneously at a high- and low-sponge-biomass ground. Our measurements show high bottom currents at both sites with distinct differences in tidal dynamics. While semidiurnal tidal harmonics predominate at both sites, tidally driven horizontal current speeds were around five times higher at HSB than at LSB. At the HSB site, barotropic and near-bottom M2 tidal currents are oriented across-slope, but the near-bottom M2 tidal ellipse is smaller in magnitude and strongly indicating enhanced local near-bottom energy dissipation of the barotropic tide through tide-topography interaction (Table 2; Fig. 8). At the LSB site, near-bottom M2 and S2 tidal ellipses from the ADCP are oriented along-slope with a small across-slope component. In contrast, modelled barotropic semi-diurnal tidal harmonics were of similar magnitude, but mainly oriented

505 across- interaction (Table 2; Fig. 8). This discrepancy is likely due to local changes in bathymetry (Fig. S1), which are not resolved in the OTIS tidal model. The outcome of strongly enhanced current speeds at the HSB site is contrary to White (2003) who measured high current speeds in areas where no sponges were recorded, and vice versa, at the Porcupine Sea Bight. Caution should be applied comparing these areas, as the sponge fields in the Porcupine Sea Bight mostly consist of glass sponges, and here we see a mixture of glass sponges and massive demosponges. Bottom current speeds are higher at HSB than
510 at LSB (Table 1), but bottom currents at LSB are still comparable with current speeds found at other sponge grounds on the Scotian Shelf (mean: 0.12 m s^{-1} ; Hanz et al., 2021a) and on the Arctic mid-Atlantic ridge (mean: 0.14 m s^{-1} ; Hanz et al., 2021b). The conversion of kinetic energy from barotropic to baroclinic tides and to turbulence over rough topography shapes the distribution of benthic filter feeding communities in many areas throughout the global ocean (van der Kaaden et al., 2024). At the northern Labrador shelf break, larger aggregations of sponges are mainly found on topographic slopes, where near-critical
515 and super-critical reflection of internal waves are predicted (Fig. 13).



520 **Figure 13: The internal wave slope parameter indicates sub-critical conditions across most of the Labrador Shelf and in the deep Northwest Atlantic. Near-critical and super-critical conditions are primarily observed along the continental margin. This analysis suggests that the HSB lander (northern point) was situated in near-critical conditions for the M2 tide, while the LSB lander (southern point) experienced supercritical bottom slopes for M2.**

4.4 How can strong bottom currents benefit the benthic community?

Strong tidally-induced bottom currents can benefit the benthic community at the HSB site in various ways. First, passive suspension feeders as the gorgonian *P. resedaeformis* benefit from high horizontal currents through an increased particulate organic matter flux (Shimeta and Jumars, 1991) and sponges (specifically glass sponges) could benefit from an increased water

525 flow rate through their body plan (Leys et al., 2011; Vogel, 1977), thereby increasing food availability. Second, resuspension
caused by oscillating tidal bottom currents enhance organic matter and inorganic nutrient availability in the benthic boundary
layer and enhance food supply to the sponges (Roberts et al., 2018). In this study, high along-slope bottom currents at both
sites were associated with increased turbidity (both ABS and OBS), indicative of resuspension. However, the beneficial effect
of resuspension for sponge biomass is not yet fully understood, as reoccurring strong turbidity flows (at LSB) could also
530 prevent high sponge biomass from developing by smothering young sponges when particles settle out (Klitgaard and Tendal,
2004).

The substrate at HSB consisted mostly of pebbles, cobbles, and boulders (Dinn et al., 2020) and a qualitative assessment of
the sediment type at LSB suggested the dominance of muddy soft sediment (Coté et al., 2019; J. Vad, *pers. com.*). As higher
bottom currents would increase bed shear stress and thereby enhance resuspension (Jones et al., 1998; Lesht, 1979), we argue
535 that fine material is resuspended at HSB before its accumulation on the seafloor. This increases availability of organic matter
to benthic suspension feeders in the benthic boundary layer and prevent smothering from sedimentation. Resuspension has
also been linked to high sponge biomass (Davison et al., 2019), as potential food sources such as organic matter and bacteria
can bind to suspended particles in the water column. The interaction of high bottom currents with rough topography causes
turbulence and mixing of bottom waters (Witte et al., 1997; Leys et al., 2011; Culwick et al., 2020). As the substrate is likely
540 rougher and bottom currents are higher at HSB than at LSB, the bottom water probably experiences more intense mixing and
turbulence at HSB. Finally, periodic supply of fresh phytoplankton derived material during the spring bloom (Fig. S10, Fig.
S11) increases the food availability of passive suspension feeders living on the sponge grounds. In short, the stronger tidal
currents at HSB enhance bottom water mixing which replenishes oxygen, dissolved organic matter, POM, and (inorganic)
nutrients in the benthic boundary layer, and thereby increases food supply to benthic fauna (Davison et al., 2019; Hanz et al.,
545 2021a, b).

4.5 Surface productivity and benthic-pelagic coupling

The Hudson Strait outflow water is known to increase nutrient concentrations in the surface waters on the northern Labrador
Shelf (Drinkwater and Harding, 2001; Kollmeyer et al., 1967; Sutcliffe et al., 1983). The increased nutrient supply supports
high primary productivity in an area extending from the Hudson Strait to the southern Labrador Shelf, bounded by the thermal
550 front associated with the 1,000 m isobath (Cyr and Larouche, 2015; Frajka-Williams et al., 2009; Frajka-Williams and Rhines,
2010). Previous studies show that surface chl-a concentrations are comparable between the two sponge grounds (see Fig. 2A
in Frajka-Williams and Rhines, 2010), suggesting that differences in surface productivity alone are insufficient to explain the
differences sponge biomass between regions. Furthermore, studies elsewhere in the Canadian Arctic have shown that benthic
biomass is explained not only by surface productivity but also by local hydrodynamics and benthic-pelagic coupling
555 (Grebmeier and Barry, 1991; Roy et al., 2014; Thomson, 1982).

Our year-long recordings of bottom water chl-a concentrations provide evidence for strong benthic-pelagic coupling during
spring in this region. The benthic landers showed early arrival of fresh phytodetritus in early March, a peak in chl-a mid-April,

and chl-a concentration was close to background values again from early May at LSB and from mid-May at HSB (Fig. 9C). Studies on the onset of the phytoplankton bloom on the Labrador Shelf show that blooms usually initiate around mid-April and peak around mid-June (Cyr et al., 2023; Frajka-Williams and Rhines, 2010; Fuentes-Yaco et al., 2007). The study of Cyr et al. (2023) estimates that the standard deviation in timing of the initiation of the phytoplankton bloom is around 21 days. As environmental conditions of the Northern Labrador Shelf were close to average during 2019 (Cyr and Galbraith, 2021), we think it's acceptable to assume phytoplankton bloom timing was similar to values found in literature. Therefore, arrival of phytodetritus at our benthic landers was then three months earlier to normal phytoplankton bloom timing. Earlier research has shown that chl-a starts to increase on the northern Labrador Shelf from early March onwards (Harrison et al., 2013). During this time the water column is still relatively cold and poorly stratified, allowing for relatively high export of phytoplankton to the seafloor. Additionally, the short periods of low ice-cover mid-February and mid-March (Fig. S11D) match the subsequent increase in bottom chl-a concentration seen for both landers (Fig. 9C). The onset of the phytoplankton bloom for the northern Labrador Shelf is around mid-April, and related to the onset of stratification (Cyr et al., 2023) and sea-ice cover (Wu et al., 2007). The timing of peak bottom chl-a concentrations (mid-April) and consequential decline compare well with the timing phytoplankton bloom initiation proposed by Cyr et al. (2023). They show there is a south-to-north progression of the phytoplankton bloom over the Labrador Shelf, which matches with our data that shows chl-a concentrations stay elevated around three weeks longer at the more northern HSB lander. Furthermore, assuming surface chl-a concentration peaks in June, we can infer that there appears to be a decoupling between pelagic productivity and bottom chl-a concentration in summer, likely due to enhanced stratification and intense zooplankton grazing (Rivkin et al., 1996; Turner, 2015). Our findings suggest strong benthic-pelagic coupling started weeks before the peak of the phytoplankton bloom, supplying fresh fluorescent material to the seafloor in spring for a period of weeks to months. Since the timing of phytoplankton bloom for high-latitude seas is shifting to earlier in the year due to rising temperatures and earlier sea-ice retreat (Edwards and Richardson, 2004; Hunter-Cevera et al., 2016; Wu et al., 2007), and since deep-sea sessile organisms, such as cold-water corals and deep-sea sponges demonstrate seasonality in their phenology (Leys and Lauzon, 1998; Maier et al., 2020b; Maldonado, 2011), the early arrival of phytoplankton-derived material could have consequences for their overall fitness and survival. Nevertheless, the effect of a shift in spring bloom timing for benthic suspension feeders, including deep-sea sponges, remains unknown.

Recent ABS measurements reveal a layer of increased 300 kHz backscatter along the northern Labrador Shelf, indicative of high abundance of micronekton and macrozooplankton (Chawarski et al., 2022). Earlier studies showed a high zooplankton biomass on the Newfoundland Shelf from July onwards (Head et al., 2003, 2013). In our traps the highest flux of unsaturated alcohols, a biomarker for zooplankton (specifically copepods; Dalsgaard et al., 2003), and the highest numbers of swimmers were in summer and autumn. During the spring bloom, trapped material at LSB had the highest relative amount of unsaturated alcohols while at HSB the level of PUFAs, markers for phytoplankton derived-material, was highest (Dalsgaard et al., 2003). Furthermore, our observations suggest that the number of trapped swimmers was higher at LSB than at HSB. These results are consistent with the hypothesis that zooplankton biomass is high over the northern Labrador Shelf (Saglek Bank) and that

zooplankton is transported by the southerly current along the Labrador Shelf together with the high phytoplankton biomass plume (Drinkwater and Harding, 2001; Sutcliffe et al., 1983). Overall, there was a larger fraction of zooplankton marker lipids in trapped material at LSB, which implies that zooplankton play a more important role in benthic-pelagic coupling at LSB than at HSB.

4.6 Organic matter fluxes to the seafloor

Organic matter deposition was higher at the HSB lander than at the LSB lander. Overall, deposition was highest during the winter months and consisted of more degraded material than during summer, indicated by high C:N ratios and high $\delta^{15}\text{N}$ values. This increased deposition in winter is likely resuspended material as shown by peaks in ABS turbidity in the bottom boundary layer and relate to higher current speeds. The C:N ratio of deposited matter was higher at LSB (~13) compared to HSB (~8), indicating the material was more degraded at LSB. Hanz et al. (2021a, 2021b) also found higher mass and carbon fluxes during winter months and low carbon fluxes when the spring/summer phytoplankton bloom arrived. They attributed this to the presence of more degraded and resuspended material in winter. Data concerning mass fluxes from sponge grounds remain scarce, but the fluxes measured here (HSB $2.46 \pm 1.76 \text{ g m}^{-2} \text{ day}^{-1}$, LSB: $1.43 \pm 0.93 \text{ g m}^{-2} \text{ day}^{-1}$) were comparable to those of a *Vazella pourtalesii* sponge ground on the Scotian Shelf ($3.17 \pm 3.42 \text{ g m}^{-2} \text{ day}^{-1}$; Hanz et al., 2021a) but substantially higher than those of a sponge ground on the Arctic mid-Atlantic ridge ($0.03 - 0.30 \text{ g m}^{-2} \text{ day}^{-1}$; Hanz et al., 2021b). Overall, our data suggest organic matter deposition fluxes are higher at HSB compared to LSB, and that the organic matter is of higher quality. The organic carbon fluxes (HSB: $3.07 \pm 1.91 \text{ mmol C m}^{-2} \text{ d}^{-1}$; LSB: $1.91 \pm 0.71 \text{ mmol C m}^{-2} \text{ d}^{-1}$) reported in our study are considerably lower than those of a more shallow (150 – 250 m depth) *V. pourtalesii* sponge ground on the Scotian Shelf ($8.3 \text{ mmol C m}^{-2} \text{ d}^{-1}$; Hanz et al., 2021a), but high compared to an Arctic mid-Atlantic ridge sponge ground (peak of $1.6 \text{ mmol C m}^{-2} \text{ d}^{-1}$; Hanz et al., 2021b). The higher organic matter deposition rate and relative fresher material at HSB compared to LSB are likely related to its shallower position on the shelf and the more dynamic water column.

4.7 Isotopic signatures of benthic macrofauna at two contrasting sponge grounds

Although the sample size was limited, the stable isotope data revealed interesting patterns of organic matter utilization by the benthic community. The gorgonian coral *P. resedaeformis* is found one trophic level (Fry, 2006) above the sediment trap material and therefore likely feeds on sinking organic matter, confirming previous observations (Sherwood et al., 2005, 2008). Sponges can generally be classified into two groups based on their associated microbial fauna, those with high microbial abundance (HMA) or those with low microbial abundance (LMA; Vacelet and Donadey, 1977). *Geodia* spp. can occur in high abundance and biomass on sponge grounds (Kutti et al., 2013). These sponges are considered HMA (Radax et al., 2012) and feed mostly on dissolved organic matter with additional particulate sources such as bacterioplankton (Bart et al., 2021). Many hexactinellidae that can form sponge grounds, for instance *Vazella pourtalesii* and *Aphrocallistes vastus*, are considered LMA sponges and feed mostly on bacterioplankton (Kahn et al., 2015). The high $\delta^{15}\text{N}$ isotopic ratios for the sponges *Asconema* spp. ($12.6 \pm 0.3 \text{ ‰ } \delta^{15}\text{N}$) and *Mycale* spp. ($13.1 \pm 0.4 \text{ ‰ } \delta^{15}\text{N}$), have been observed previously for LMA sponges (Iken et al., 2001;

Kahn et al., 2018; Polunin, 2001). Deep-sea LMA sponges typically have elevated $\delta^{15}\text{N}$ values in the benthic food web (Kahn et al., 2018), a phenomenon that is still poorly understood. Possible explanations could be selective feeding on ^{15}N enriched bacteria (Wilkinson et al., 1984), feeding on resuspended benthic bacteria (Kahn et al., 2018), or nitrogen (re)cycling within the sponge holobiont (Hanz et al., 2022; Rooks et al., 2020). Interestingly, the HMA massive sponge *Geodia* sp. has distinct $\delta^{13}\text{C}$ and $\delta^{15}\text{N}$ values, which was also observed in Hanz et al. (2022), indicating different feeding or metabolic strategies. Recent research on *Geodia baretii* has indeed demonstrated that these sponges rely in large part on DOM for their metabolic requirements (Bart et al., 2021; de Kluijver et al., 2021). In this study, *Geodia* spp. ($8.2 \pm 0.2 \text{‰ } \delta^{15}\text{N}$) was one trophic level higher than oceanic DOM $\delta^{15}\text{N}$ ($\sim 5 \text{‰}$; Benner et al., 2005; Sigman et al., 2009) and $\delta^{15}\text{N-NO}_3^-$ ($\sim 5 \text{‰}$; Sigman et al., 2009; Sherwood et al., 2021), limiting our ability to distinguish between DOM and NO_3^- (by i.e., denitrification; Hoffmann et al., 2009) as potential nitrogen sources. The $\delta^{13}\text{C}$ value of *Geodia* spp. ($-18.4 \pm 0.17 \text{‰ } \delta^{13}\text{C}$) is $\pm 3.5 \text{‰}$ higher than bottom water $\delta^{13}\text{C-DOC}$ values on the Labrador Shelf (Barber et al., 2017), i.e. more than four times higher than the expected $0.8 \text{‰ } \delta^{13}\text{C}$ step per trophic level (Vander Zanden and Rasmussen, 2001). Alternatively, *Geodia* spp. could capitalize on DIC via their symbionts (de Kluijver et al., 2021), as recently observed in Arctic *Geodia* spp. assemblages (Morganti et al., 2022) and other deep-sea sponges (van Duyl et al., 2020). Even limited chemoautotrophic assimilation of high $\delta^{13}\text{C-DIC}$ ($\sim 0 \text{‰ } \delta^{13}\text{C}$) could explain the high $\delta^{13}\text{C}$ values of *Geodia* spp. These results indicate that passive suspension feeders benefit from high tidal currents through an increased particulate organic matter flux (Shimeta and Jumars, 1991), whereas sponges likely benefit from replenishment of nutrients, oxygen, and dissolved organic matter (Schl ppy et al., 2010).

5 Conclusion

The aim this research was to obtain a better understanding of the environmental conditions in which sponge grounds occur and investigate the conditions in which high-sponge-biomass could develop. This study identified that the high-biomass sponge ground on the northern Labrador Shelf differ from the low-biomass sponge ground in the following ways: a more dynamic water column with strong tidal bottom currents and near-bottom energy dissipation by tide-topography interactions, increased bottom inorganic nutrient concentrations, and higher organic matter flux to the seafloor. Furthermore, both sponge grounds experienced strong benthic-pelagic coupling during spring and a decoupling during summer months. The elevated bottom nutrient concentrations at the high-sponge-biomass ground could be related to large scale circulation or sediment effluxes, and future work is needed to assess this. Our findings suggest a relation between slope-criticality and sponge biomass on the northern Labrador Shelf which could be interesting to investigate in future work. The deep-sea sponges and corals benefit from the dynamic water column in the high-biomass sponge ground by increased availability of food sources and nutrients.

6 Funding statement

This research was supported by the European Union's Horizon 2020 Research and Innovation Programme under grant agreement nos. 678760 (ATLAS) and 818123 (iAtlantic). This output reflects only the authors' view, and the European Union cannot be held responsible for any use that may be made of the information contained therein. Department of Fisheries and Oceans contributions were funded through the departmental International Governance Strategy programme awarded to EK. DvO was supported by the Innovational Research Incentives Scheme of the Netherlands Organisation for Scientific Research (NWO), respectively, under grant agreement 864.13.007. EdF was partly supported by ArcticNet Network of Centres of Excellence, Glacier troughs as biodiversity and abundance hotspots in Arctic and subarctic regions project, ArcticNet Phase V (Geoffroy et al.). The data presented herein were collected by the Canadian research icebreaker CCGS Amundsen and made available by the Amundsen Science program, which was supported by the Canada Foundation for Innovation and Natural Sciences and Engineering Research Council of Canada. The views expressed in this publication do not necessarily represent the views of Amundsen Science or that of its partners. Ship-time on the CCGS Amundsen was also funded by an NSERC ship-time grant (Edinger et al., grant nr.: RGPST-515528-2018), ArcticNet Network of Centers of Excellence Canada, and the Department of Fisheries and Oceans Canada (DFO; Coté et al.). The funders had no role in study design, data collection, and analysis, decision to publish, or preparation of the manuscript.

7 Author statement

EDF: sample analysis, data analysis, and writing; IY: data collection, data analysis, and writing. CM: conceptualization, data analysis and writing; JV: data collection and data analysis; FM: conceptualization, sample analysis and data analysis; GD: conceptualization, data analysis; EK, EH, IY, SWR, MR: conceptualization and site selection; SWR, MR, EK, BM, GT: site contribution and preparation of benthic landers; GW: conceptualization, sample analysis, data analysis, and writing; SB: data collection and sample analysis; DvO: conceptualization, data analysis, writing. All authors contributed to the article and approved the submitted version.

8 Acknowledgements

We would like to thank the skillful crew and technicians on board CCGS Amundsen for their support during the fieldwork. Specifically, we thank Dr. Paul Snelgrove (Memorial University of Newfoundland), Dr. Evan Edinger (Memorial University of Newfoundland), Dr. David Cote (DFO) and Shawn Meredyk (Amundsen Science) for their assistance in facilitating our field programme. Cam Lirette (DFO) assisted in preparing various data layers to assist in site selection. We would also like to thank Jan Peene for nutrient analysis, Peter van Breugel and Jurian Brasser for help in measuring macrofauna/POM/sediment trap stable isotopes, and Pascal Guillot for quality assurance of the CTD profiles. Finally, we thank Kevin MacIsaac and Marc Ringuette for their help in identifying the sediment trap swimmers.

9 Data availability

Data is available at: <https://doi.org/10.5281/zenodo.10571403>

10 Competing interest statement

685 The authors declare that they have no conflict of interest.

11 References

- Abelson, A. and Denny, M.: Settlement of Marine Organisms in Flow, *Annu. Rev. Ecol. Syst.*, 28, 317–339, <https://doi.org/10.1146/annurev.ecolsys.28.1.317>, 1997.
- 690 Andrews, D. and Hargrave, B. T.: Close interval sampling of interstitial silicate and porosity in marine sediments, *Geochimica et Cosmochimica Acta*, 48, 711–722, [https://doi.org/10.1016/0016-7037\(84\)90097-8](https://doi.org/10.1016/0016-7037(84)90097-8), 1984.
- Barber, A., Sirois, M., Chaillou, G., and Gélinas, Y.: Stable isotope analysis of dissolved organic carbon in Canada’s eastern coastal waters, *Limnology and Oceanography*, 62, S71–S84, <https://doi.org/10.1002/lno.10666>, 2017.
- Bart, M. C., Mueller, B., Rombouts, T., van de Ven, C., Tompkins, G. J., Osinga, R., Brussaard, C. P. D., MacDonald, B.,
695 Engel, A., Rapp, H. T., and de Goeij, J. M.: Dissolved organic carbon (DOC) is essential to balance the metabolic demands of four dominant North-Atlantic deep-sea sponges, *Limnology and Oceanography*, 66, 925–938, <https://doi.org/10.1002/lno.11652>, 2021.
- Beazley, L., Wang, Z., Kenchington, E., Yashayaev, I., Rapp, H. T., Xavier, J. R., Murillo, F. J., Fenton, D., and Fuller, S.:
700 Predicted distribution of the glass sponge *Vazella pourtalesi* on the Scotian Shelf and its persistence in the face of climatic variability, *PLOS ONE*, 13, e0205505, <https://doi.org/10.1371/journal.pone.0205505>, 2018.
- Beazley, L., Kenchington, E., Murillo, F., Brickman, D., Wang, Z., Davies, A., Roberts, E., and Rapp, H.: Climate change winner in the deep sea? Predicting the impacts of climate change on the distribution of the glass sponge *Vazella pourtalesii*, *Mar. Ecol. Prog. Ser.*, 657, 1–23, <https://doi.org/10.3354/meps13566>, 2021.
- 705 Beazley, L. I., Kenchington, E. L., Murillo, F. J., and Sacau, M. del M.: Deep-sea sponge grounds enhance diversity and abundance of epibenthic megafauna in the Northwest Atlantic, *ICES Journal of Marine Science*, 70, 1471–1490, <https://doi.org/10.1093/icesjms/fst124>, 2013.
- Becker, O. S. code by R. A. and Brownrigg, A. R. W. R. version by R.: mapdata: Extra Map Databases, 2022.
- Belkin, I. M.: Rapid warming of Large Marine Ecosystems, *Progress in Oceanography*, 81, 207–213, <https://doi.org/10.1016/j.pocean.2009.04.011>, 2009.
- 710 Benner, R., Louchouart, P., and Amon, R. M. W.: Terrigenous dissolved organic matter in the Arctic Ocean and its transport to surface and deep waters of the North Atlantic, *Global Biogeochemical Cycles*, 11, 2005.
- Bergquist, P. R.: Sponges, University of California Press, 282 pp., 1978.

- Bloomfield, P.: *Fourier analysis of time series: an introduction*, John Wiley & Sons, 2004.
- 715 Brito-Morales, I., Schoeman, D. S., Molinos, J. G., Burrows, M. T., Klein, C. J., Arafeh-Dalmau, N., Kaschner, K., Garilao, C., Kesner-Reyes, K., and Richardson, A. J.: Climate velocity reveals increasing exposure of deep-ocean biodiversity to future warming, *Nat. Clim. Chang.*, 10, 576–581, <https://doi.org/10.1038/s41558-020-0773-5>, 2020.
- Brodnicke, O. B., Meyer, H. K., Busch, K., Xavier, J. R., Knudsen, S. W., Møller, P. R., Hentschel, U., and Sweet, M. J.: Deep-sea sponge derived environmental DNA analysis reveals demersal fish biodiversity of a remote Arctic ecosystem, *Environmental DNA*, 5, 1405–1417, <https://doi.org/10.1002/edn3.451>, 2023.
- 720 Buhl-Mortensen, L., Vanreusel, A., Gooday, A. J., Levin, L. A., Priede, I. G., Buhl-Mortensen, P., Gheerardyn, H., King, N. J., and Raes, M.: Biological structures as a source of habitat heterogeneity and biodiversity on the deep ocean margins, *Marine Ecology*, 31, 21–50, <https://doi.org/10.1111/j.1439-0485.2010.00359.x>, 2010.
- Campitelli, E.: *metR: Tools for Easier Analysis of Meteorological Fields*, <https://doi.org/10.5281/zenodo.2593516>, 2021.
- 725 Latest Ice conditions: <https://www.canada.ca/en/environment-climate-change/services/ice-forecasts-observations/latest-conditions.html>, last access: 2 January 2022.
- Cathalot, C., Van Oevelen, D., Cox, T. J. S., Kutti, T., Lavaleye, M., Duineveld, G., and Meysman, F. J. R.: Cold-water coral reefs and adjacent sponge grounds: hotspots of benthic respiration and organic carbon cycling in the deep sea, *Front. Mar. Sci.*, 2, <https://doi.org/10.3389/fmars.2015.00037>, 2015.
- 730 Centurioni, L. R., Turton, J., Lumpkin, R., Braasch, L., Brassington, G., Chao, Y., Charpentier, E., Chen, Z., Corlett, G., Dohan, K., Donlon, C., Gallage, C., Hormann, V., Ignatov, A., Ingleby, B., Jensen, R., Kelly-Gerreyn, B. A., Koszalka, I. M., Lin, X., Lindstrom, E., Maximenko, N., Merchant, C. J., Minnett, P., O’Carroll, A., Paluszkiwicz, T., Poli, P., Poulain, P.-M., Reverdin, G., Sun, X., Swail, V., Thurston, S., Wu, L., Yu, L., Wang, B., and Zhang, D.: Global in situ Observations of Essential Climate and Ocean Variables at the Air–Sea Interface, *Front. Mar. Sci.*, 6, <https://doi.org/10.3389/fmars.2019.00419>, 2019.
- 735 Chawarski, J., Klevjer, T., Coté, D., and Geoffroy, M.: The transformation of mesopelagic structure across polar fronts, *Research Square*, <https://doi.org/10.21203/rs.3.rs-244272/v1>, 2022.
- Christie, W. W.: A simple procedure for rapid transmethylolation of glycerolipids and cholesteryl esters, *Journal of Lipid Research*, 23, 1072–1075, [https://doi.org/10.1016/S0022-2275\(20\)38081-0](https://doi.org/10.1016/S0022-2275(20)38081-0), 1982.
- 740 Colaço, A., Rapp, H. T., Companyà-Llovet, N., and Pham, C. K.: Bottom trawling in sponge grounds of the Barents Sea (Arctic Ocean): A functional diversity approach, *Deep Sea Research Part I: Oceanographic Research Papers*, 183, 103742, <https://doi.org/10.1016/j.dsr.2022.103742>, 2022.
- Coté, D., Edinger, E. N., and Mercier, A.: *CCGS Amundsen Field Report. Integrated studies and ecosystem characterization of the Labrador Sea Deep Ocean (ISECOLD)*., 2018.
- 745 Coté, D., Geoffroy, M., Sherwood, O. A., Neves, B. M., Mercier, A., Hubert, C., Dukhovskoy, D., and Vad, J.: *CCGS Amundsen Field Report. Integrated studies and ecosystem characterization of the Labrador Sea Deep Ocean (ISECOLD)*., 2019.
- Culwick, T., Phillips, J., Goodwin, C., Rayfield, E. J., and Hendry, K. R.: Sponge Density and Distribution Constrained by Fluid Forcing in the Deep Sea, *Front. Mar. Sci.*, 7, 395, <https://doi.org/10.3389/fmars.2020.00395>, 2020.

- 750 Cuny, J., Rhines, P. B., Niiler, P. P., and Bacon, S.: Labrador Sea Boundary Currents and the Fate of the Irminger Sea Water, *Journal of Physical Oceanography*, 32, 627–647, [https://doi.org/10.1175/1520-0485\(2002\)032<0627:LSBCAT>2.0.CO;2](https://doi.org/10.1175/1520-0485(2002)032<0627:LSBCAT>2.0.CO;2), 2002.
- Curry, B., Lee, C. M., and Petrie, B.: Volume, Freshwater, and Heat Fluxes through Davis Strait, 2004–05, *Journal of Physical Oceanography*, 41, 429–436, <https://doi.org/10.1175/2010JPO4536.1>, 2011.
- 755 Curry, B., Lee, C. M., Petrie, B., Moritz, R. E., and Kwok, R.: Multiyear Volume, Liquid Freshwater, and Sea Ice Transports through Davis Strait, 2004–10, *Journal of Physical Oceanography*, 44, 1244–1266, <https://doi.org/10.1175/JPO-D-13-0177.1>, 2014.
- Cyr, F. and Galbraith, P. S.: A climate index for the Newfoundland and Labrador shelf, *Earth System Science Data*, 13, 1807–1828, <https://doi.org/10.5194/essd-13-1807-2021>, 2021.
- 760 Cyr, F. and Larouche, P.: Thermal Fronts Atlas of Canadian Coastal Waters, *Atmosphere-Ocean*, 53, 212–236, <https://doi.org/10.1080/07055900.2014.986710>, 2015.
- Cyr, F., Lewis, K., Bélanger, D., Regular, P., Clay, S., and Devred, E.: Physical controls and ecological implications of the timing of the spring phytoplankton bloom on the Newfoundland and Labrador shelf, *Limnology and Oceanography Letters*, n/a, <https://doi.org/10.1002/lol2.10347>, 2023.
- 765 Dalsgaard, J., St. John, M., Kattner, G., Müller-Navarra, D., and Hagen, W.: Fatty acid trophic markers in the pelagic marine environment, in: *Advances in Marine Biology*, vol. 46, Elsevier, 225–340, [https://doi.org/10.1016/S0065-2881\(03\)46005-7](https://doi.org/10.1016/S0065-2881(03)46005-7), 2003.
- Davison, J. J., van Haren, H., Hosegood, P., Piechaud, N., and Howell, K. L.: The distribution of deep-sea sponge aggregations (Porifera) in relation to oceanographic processes in the Faroe-Shetland Channel, *Deep Sea Research Part I: Oceanographic Research Papers*, 146, 55–61, <https://doi.org/10.1016/j.dsr.2019.03.005>, 2019.
- 770 Dinn, C., Zhang, X., Edinger, E., and Leys, S. P.: Sponge communities in the eastern Canadian Arctic: species richness, diversity and density determined using targeted benthic sampling and underwater video analysis, *Polar Biol*, 43, 1287–1305, <https://doi.org/10.1007/s00300-020-02709-z>, 2020.
- Drinkwater, K. F. and Harding, G. C.: Effects of the Hudson Strait outflow on the biology of the Labrador Shelf, *Can. J. Fish. Aquat. Sci.*, 58, 171–184, <https://doi.org/10.1139/f00-210>, 2001.
- 775 Drinkwater, K. F. and Jones, E. P.: Density stratification, nutrient and chlorophyll distributions in the Hudson Strait region during summer and their relation to tidal mixing, *Continental Shelf Research*, 7, 599–607, [https://doi.org/10.1016/0278-4343\(87\)90025-2](https://doi.org/10.1016/0278-4343(87)90025-2), 1987.
- 780 Dunbar, M. J.: Eastern Arctic waters: a summary of our present knowledge of the physical oceanography of the eastern arctic area, from Hudson bay to cape Farewell and from Bell Isle to Smith sound, *Fisheries Research Board of Canada*, Ottawa, 131 pp., 1951.
- van Duyl, F. C., Lengger, S. K., Schouten, S., Lundälv, T., van Oevelen, D., and Müller, C. E.: Dark CO₂ fixation into phospholipid-derived fatty acids by the cold-water coral associated sponge *Hymedesmia (Stylopus) coriacea* (Tisler Reef, NE Skagerrak), *Marine Biology Research*, 1–17, <https://doi.org/10.1080/17451000.2019.1704019>, 2020.

- 785 van Duyl, F., Hegeman, J., Hoogstraten, A., and Maier, C.: Dissolved carbon fixation by sponge–microbe consortia of deep water coral mounds in the northeastern Atlantic Ocean, *Mar. Ecol. Prog. Ser.*, 358, 137–150, <https://doi.org/10.3354/meps07370>, 2008.
- Edwards, M. and Richardson, A. J.: Impact of climate change on marine pelagic phenology and trophic mismatch, *Nature*, 430, 881–884, <https://doi.org/10.1038/nature02808>, 2004.
- 790 Egbert, G. D. and Erofeeva, S. Y.: Efficient Inverse Modeling of Barotropic Ocean Tides, *Journal of Atmospheric and Oceanic Technology*, 19, 183–204, [https://doi.org/10.1175/1520-0426\(2002\)019<0183:EIMOBO>2.0.CO;2](https://doi.org/10.1175/1520-0426(2002)019<0183:EIMOBO>2.0.CO;2), 2002.
- Elipot, S., Lumpkin, R., Perez, R. C., Lilly, J. M., Early, J. J., and Sykulski, A. M.: A global surface drifter data set at hourly resolution, *Journal of Geophysical Research: Oceans*, 121, 2937–2966, <https://doi.org/10.1002/2016JC011716>, 2016.
- Elipot, S., Sykulski, A. M., Lumpkin, R., Centurioni, L. R., and Pazos, M.: Hourly location, current velocity, and temperature collected from Global Drifter Program drifters world-wide., 2022.
- 795 Fissel, D. B. and Lemon, D. D.: Analysis of physical oceanographic data from the Labrador Shelf, summer 1980, 1991.
- Frajka-Williams, E. and Rhines, P. B.: Physical controls and interannual variability of the Labrador Sea spring phytoplankton bloom in distinct regions, *Deep Sea Research Part I: Oceanographic Research Papers*, 57, 541–552, <https://doi.org/10.1016/j.dsr.2010.01.003>, 2010.
- 800 Frajka-Williams, E., Rhines, P. B., and Eriksen, C. C.: Physical controls and mesoscale variability in the Labrador Sea spring phytoplankton bloom observed by Seaglider, *Deep Sea Research Part I: Oceanographic Research Papers*, 56, 2144–2161, <https://doi.org/10.1016/j.dsr.2009.07.008>, 2009.
- Fry, B.: *Stable Isotope Ecology*, Springer-Verlag, New York, <https://doi.org/10.1007/0-387-33745-8>, 2006.
- 805 Fuentes-Yaco, C., Koeller, P. A., Sathyendranath, S., and Platt, T.: Shrimp (*Pandalus borealis*) growth and timing of the spring phytoplankton bloom on the Newfoundland–Labrador Shelf, *Fisheries Oceanography*, 16, 116–129, <https://doi.org/10.1111/j.1365-2419.2006.00402.x>, 2007.
- GEBCO Bathymetric Compilation Group: The GEBCO_2023 Grid - a continuous terrain model of the global oceans and land., <https://doi.org/10.5285/f98b053b-0cbc-6c23-e053-6c86abc0af7b>, 2023.
- Gille, S. T., Metzger, E. J., and Tokmakian: *Seafloor Topography and Ocean Circulation*, *Oceanography*, 2004.
- 810 Grebmeier, J. M. and Barry, J. P.: The influence of oceanographic processes on pelagic-benthic coupling in polar regions: A benthic perspective, *Journal of Marine Systems*, 2, 495–518, [https://doi.org/10.1016/0924-7963\(91\)90049-Z](https://doi.org/10.1016/0924-7963(91)90049-Z), 1991.
- Griffiths, D. K., Pingree, R. D., and Sinclair, M.: Summer tidal fronts in the near-arctic regions of Foxe Basin and Hudson Bay, *Deep Sea Research Part A. Oceanographic Research Papers*, 28, 865–873, [https://doi.org/10.1016/S0198-0149\(81\)80006-4](https://doi.org/10.1016/S0198-0149(81)80006-4), 1981.
- Grolemund, G. and Wickham, H.: Dates and Times Made Easy with lubridate, *Journal of Statistical Software*, 40, 1–25, 2011.
- 815 Guillot, P.: Cruise Bright/SN/Atlas 1802 (leg 2) CTD processing notes, Amundsen Science, 2018.

- Haalboom, S., de Stigter, H., Duineveld, G., van Haren, H., Reichart, G.-J., and Mienis, F.: Suspended particulate matter in a submarine canyon (Whittard Canyon, Bay of Biscay, NE Atlantic Ocean): Assessment of commonly used instruments to record turbidity, *Marine Geology*, 434, 106439, <https://doi.org/10.1016/j.margeo.2021.106439>, 2021.
- 820 Haalboom, S., de Stigter, H. C., Mohn, C., Vandorpe, T., Smit, M., de Jonge, L., and Reichart, G.-J.: Monitoring of a sediment plume produced by a deep-sea mining test in shallow water, Málaga Bight, Alboran Sea (southwestern Mediterranean Sea), *Marine Geology*, 456, 106971, <https://doi.org/10.1016/j.margeo.2022.106971>, 2023.
- Hanz, U., Roberts, E. M., Duineveld, G., Davies, A., Haren, H. van, Rapp, H. T., Reichart, G.-J., and Mienis, F.: Long-term Observations Reveal Environmental Conditions and Food Supply Mechanisms at an Arctic Deep-Sea Sponge Ground, *Journal of Geophysical Research: Oceans*, 126, e2020JC016776, <https://doi.org/10.1029/2020JC016776>, 2021a.
- 825 Hanz, U., Beazley, L., Kenchington, E., Duineveld, G., Rapp, H. T., and Mienis, F.: Seasonal Variability in Near-bed Environmental Conditions in the *Vazella pourtalesii* Glass Sponge Grounds of the Scotian Shelf, *Front. Mar. Sci.*, 7, 597682, <https://doi.org/10.3389/fmars.2020.597682>, 2021b.
- 830 Hanz, U., Riekenberg, P., de Kluijver, A., van der Meer, M., Middelburg, J. J., de Goeij, J. M., Bart, M. C., Wurz, E., Colaço, A., Duineveld, G. C. A., Reichart, G.-J., Rapp, H.-T., and Mienis, F.: The important role of sponges in carbon and nitrogen cycling in a deep-sea biological hotspot, *Functional Ecology*, 36, 2188–2199, <https://doi.org/10.1111/1365-2435.14117>, 2022.
- Harrison, G. W., Yngve Børsheim, K., Li, W. K. W., Maillet, G. L., Pepin, P., Sakshaug, E., Skogen, M. D., and Yeats, P. A.: Phytoplankton production and growth regulation in the Subarctic North Atlantic: A comparative study of the Labrador Sea-Labrador/Newfoundland shelves and Barents/Norwegian/Greenland seas and shelves, *Progress in Oceanography*, 114, 26–45, <https://doi.org/10.1016/j.pocean.2013.05.003>, 2013.
- 835 Head, E. J. H., Harris, L. R., and Yashayaev, I.: Distributions of *Calanus* spp. and other mesozooplankton in the Labrador Sea in relation to hydrography in spring and summer (1995–2000), *Progress in Oceanography*, 59, 1–30, [https://doi.org/10.1016/S0079-6611\(03\)00111-3](https://doi.org/10.1016/S0079-6611(03)00111-3), 2003.
- Head, E. J. H., Melle, W., Pepin, P., Bagøien, E., and Broms, C.: On the ecology of *Calanus finmarchicus* in the Subarctic North Atlantic: A comparison of population dynamics and environmental conditions in areas of the Labrador Sea-Labrador/Newfoundland Shelf and Norwegian Sea Atlantic and Coastal Waters, *Progress in Oceanography*, 114, 46–63, <https://doi.org/10.1016/j.pocean.2013.05.004>, 2013.
- 840 Hoffmann, F., Radax, R., Woebken, D., Holtappels, M., Lavik, G., Rapp, H. T., Schläppy, M.-L., Schleper, C., and Kuypers, M. M. M.: Complex nitrogen cycling in the sponge *Geodia barretti*, *Environmental Microbiology*, 11, 2228–2243, <https://doi.org/10.1111/j.1462-2920.2009.01944.x>, 2009.
- 845 Hogg, M., Tendal, O., Conway, K., Pomponi, S., Gutt, J., Krautter, M., Roberts, J., and others: Deep-sea sponge grounds: Reservoirs of biodiversity, 2010.
- Howell, K.-L., Piechaud, N., Downie, A.-L., and Kenny, A.: The distribution of deep-sea sponge aggregations in the North Atlantic and implications for their effective spatial management, *Deep Sea Research Part I: Oceanographic Research Papers*, 115, 309–320, <https://doi.org/10.1016/j.dsr.2016.07.005>, 2016.
- 850 Hunter-Cevera, K. R., Neubert, M. G., Olson, R. J., Solow, A. R., Shalapyonok, A., and Sosik, H. M.: Physiological and ecological drivers of early spring blooms of a coastal phytoplankter, *Science*, 354, 326–329, <https://doi.org/10.1126/science.aaf8536>, 2016.

- 855 Iken, K., Brey, T., Wand, U., Voigt, J., and Junghans, P.: Food web structure of the benthic community at the Porcupine Abyssal Plain (NE Atlantic): a stable isotope analysis, *Progress in Oceanography*, 50, 383–405, [https://doi.org/10.1016/S0079-6611\(01\)00062-3](https://doi.org/10.1016/S0079-6611(01)00062-3), 2001.
- Jones, E. P., Dyrssen, D., and Coote, A. R.: Nutrient Regeneration in Deep Baffin Bay with Consequences for Measurements of the Conservative Tracer NO and Fossil Fuel CO₂ in the Oceans, *Can. J. Fish. Aquat. Sci.*, 41, 30–35, <https://doi.org/10.1139/f84-003>, 1984.
- 860 Jones, S. E., Jago, C. F., Bale, A. J., Chapman, D., Howland, R. J. M., and Jackson, J.: Aggregation and resuspension of suspended particulate matter at a seasonally stratified site in the southern North Sea: physical and biological controls, *Continental Shelf Research*, 18, 1283–1309, [https://doi.org/10.1016/S0278-4343\(98\)00044-2](https://doi.org/10.1016/S0278-4343(98)00044-2), 1998.
- Jorda, G., Marbà, N., Bennett, S., Santana-Garcon, J., Agusti, S., and Duarte, C. M.: Ocean warming compresses the three-dimensional habitat of marine life, *Nat Ecol Evol*, 4, 109–114, <https://doi.org/10.1038/s41559-019-1058-0>, 2020.
- 865 van der Kaaden, A.-S., van Oevelen, D., Mohn, C., Soetaert, K., Rietkerk, M., van de Koppel, J., and Gerkema, T.: Resemblance of the global depth distribution of internal-tide generation and cold-water coral occurrences, *Ocean Science*, 20, 569–587, <https://doi.org/10.5194/os-20-569-2024>, 2024.
- Kahn, A. S., Yahel, G., Chu, J. W. F., Tunnicliffe, V., and Leys, S. P.: Benthic grazing and carbon sequestration by deep-water glass sponge reefs: Deep-water glass sponge reefs, *Limnol. Oceanogr.*, 60, 78–88, <https://doi.org/10.1002/lno.10002>, 2015.
- 870 Kahn, A. S., Chu, J. W. F., and Leys, S. P.: Trophic ecology of glass sponge reefs in the Strait of Georgia, British Columbia, *Sci Rep*, 8, 756, <https://doi.org/10.1038/s41598-017-19107-x>, 2018.
- Kazanidis, G., van Oevelen, D., Veuger, B., and Witte, U. F. M.: Unravelling the versatile feeding and metabolic strategies of the cold-water ecosystem engineer *Spongosorites coralliophaga* (Stephens, 1915), *Deep Sea Research Part I: Oceanographic Research Papers*, 141, 71–82, <https://doi.org/10.1016/j.dsr.2018.07.009>, 2018.
- Kelley, D. and Richards, C.: *oce: Analysis of Oceanographic Data*, 2020.
- 875 Kenchington, E., Power, D., and Koen-Alonso, M.: Associations of demersal fish with sponge grounds on the continental slopes of the northwest Atlantic, *Mar. Ecol. Prog. Ser.*, 477, 217–230, <https://doi.org/10.3354/meps10127>, 2013.
- Kenchington, E., Yashayaev, I., Tendal, O. S., and Jørgensbye, H.: Water mass characteristics and associated fauna of a recently discovered *Lophelia pertusa* (Scleractinia: Anthozoa) reef in Greenlandic waters, *Polar Biol*, 40, 321–337, <https://doi.org/10.1007/s00300-016-1957-3>, 2017.
- 880 Kenchington, E. L., Lirette, C., Cogswell, A., Archambault, D., Archambault, P., Benoit, H., Bernier, D., Brodie, B., Fuller, S., Gilkinson, K., Lévesque, M., Power, D., Siferd, T., Treble, M., and Wareham, V.: Delineating Coral and Sponge Concentrations in the Biogeographic Regions of the East Coast of Canada Using Spatial Analyses, *DFO Can. Sci. Advis. Sec. Res. Doc.*, vi + 202 pp, 2010.
- 885 Kieke, D. and Yashayaev, I.: Studies of Labrador Sea Water formation and variability in the subpolar North Atlantic in the light of international partnership and collaboration, *Progress in Oceanography*, 132, 220–232, <https://doi.org/10.1016/j.pocean.2014.12.010>, 2015.
- Kiriakoulakis, K., Bett, B. J., White, M., and Wolff, G. A.: Organic biogeochemistry of the Darwin Mounds, a deep-water coral ecosystem, of the NE Atlantic, *Deep Sea Research Part I: Oceanographic Research Papers*, 51, 1937–1954, <https://doi.org/10.1016/j.dsr.2004.07.010>, 2004.

- 890 Klitgaard, A. B.: The fauna associated with outer shelf and upper slope sponges (Porifera, Demospongiae) at the Faroe Islands, northeastern Atlantic, *Sarsia*, 80, 1–22, <https://doi.org/10.1080/00364827.1995.10413574>, 1995.
- Klitgaard, A. B. and Tendal, O. S.: Distribution and species composition of mass occurrences of large-sized sponges in the northeast Atlantic, *Progress in Oceanography*, 61, 57–98, <https://doi.org/10.1016/j.pocean.2004.06.002>, 2004.
- 895 de Kluijver, A., Bart, M. C., van Oevelen, D., de Goeij, J. M., Leys, S. P., Maier, S. R., Maldonado, M., Soetaert, K., Verbiest, S., and Middelburg, J. J.: An Integrative Model of Carbon and Nitrogen Metabolism in a Common Deep-Sea Sponge (*Geodia barretti*), *Frontiers in Marine Science*, 7, 1131, <https://doi.org/10.3389/fmars.2020.596251>, 2021.
- Knudby, A., Kenchington, E., and Murillo, F. J.: Modeling the Distribution of *Geodia* Sponges and Sponge Grounds in the Northwest Atlantic, *PLoS ONE*, 8, e82306, <https://doi.org/10.1371/journal.pone.0082306>, 2013.
- 900 Kollmeyer, R. C., United States. Coast Guard. Oceanographic Unit, McGill, D. A. (David A.), and Corwin, N.: Oceanography of the Labrador Sea in the vicinity of Hudson Strait in 1965, Washington, D.C. : U.S. Coast Guard Oceanographic Unit, 108 pp., 1967.
- Kutti, T., Bannister, R. J., and Fosså, J. H.: Community structure and ecological function of deep-water sponge grounds in the Traenadypet MPA—Northern Norwegian continental shelf, *Continental Shelf Research*, 69, 21–30, <https://doi.org/10.1016/j.csr.2013.09.011>, 2013.
- 905 Kutti, T., Fosså, J., and Bergstad, O.: Influence of structurally complex benthic habitats on fish distribution, *Mar. Ecol. Prog. Ser.*, 520, 175–190, <https://doi.org/10.3354/meps11047>, 2015.
- Lazier, J., Hendry, R., Clarke, A., Yashayaev, I., and Rhines, P.: Convection and restratification in the Labrador Sea, 1990–2000, *Deep Sea Research Part I: Oceanographic Research Papers*, 49, 1819–1835, [https://doi.org/10.1016/S0967-0637\(02\)00064-X](https://doi.org/10.1016/S0967-0637(02)00064-X), 2002.
- 910 Lehmann, N., Kienast, M., Granger, J., Bourbonnais, A., Altabet, M. A., and Tremblay, J.-É.: Remote Western Arctic Nutrients Fuel Remineralization in Deep Baffin Bay, *Global Biogeochemical Cycles*, 33, 649–667, <https://doi.org/10.1029/2018GB006134>, 2019.
- Lesht, B. M.: Relationship between sediment resuspension and the statistical frequency distribution of bottom shear stress, *Marine Geology*, 32, M19–M27, [https://doi.org/10.1016/0025-3227\(79\)90142-7](https://doi.org/10.1016/0025-3227(79)90142-7), 1979.
- 915 Leys, S. P. and Lauzon, N. R. J.: Hexactinellid sponge ecology: growth rates and seasonality in deep water sponges, *Journal of Experimental Marine Biology and Ecology*, 230, 111–129, [https://doi.org/10.1016/S0022-0981\(98\)00088-4](https://doi.org/10.1016/S0022-0981(98)00088-4), 1998.
- Leys, S. P., Yahel, G., Reidenbach, M. A., Tunnicliffe, V., Shavit, U., and Reiswig, H. M.: The Sponge Pump: The Role of Current Induced Flow in the Design of the Sponge Body Plan, *PLoS ONE*, 6, e27787, <https://doi.org/10.1371/journal.pone.0027787>, 2011.
- 920 López-Acosta, M., Leynaert, A., and Maldonado, M.: Silicon consumption in two shallow-water sponges with contrasting biological features, *Limnology and Oceanography*, 61, 2139–2150, <https://doi.org/10.1002/lno.10359>, 2016.
- Lovelace, R., Félix, R., and Talbot, J.: slopes: Calculate Slopes of Roads, Rivers and Trajectories, 2022.
- Maier, S. R., Kutti, T., Bannister, R. J., Fang, J. K.-H., van Breugel, P., van Rijswijk, P., and van Oevelen, D.: Recycling pathways in cold-water coral reefs: Use of dissolved organic matter and bacteria by key suspension feeding taxa, *Scientific Reports*, 10, 9942, <https://doi.org/10.1038/s41598-020-66463-2>, 2020a.
- 925

- Maier, S. R., Bannister, R. J., van Oevelen, D., and Kutti, T.: Seasonal controls on the diet, metabolic activity, tissue reserves and growth of the cold-water coral *Lophelia pertusa*, *Coral Reefs*, 39, 173–187, <https://doi.org/10.1007/s00338-019-01886-6>, 2020b.
- Maldonado, M.: The ecology of the sponge larva, *Canadian Journal of Zoology*, <https://doi.org/10.1139/z05-177>, 2011.
- 930 Maldonado, M., Navarro, L., Grasa, A., Gonzalez, A., and Vaquerizo, I.: Silicon uptake by sponges: a twist to understanding nutrient cycling on continental margins, *Sci Rep*, 1, 30, <https://doi.org/10.1038/srep00030>, 2011.
- Maldonado, M., Ribes, M., and van Duyl, F. C.: Nutrient Fluxes Through Sponges, in: *Advances in Marine Biology*, vol. 62, Elsevier, 113–182, <https://doi.org/10.1016/B978-0-12-394283-8.00003-5>, 2012.
- 935 Maldonado, M., López-Acosta, M., Beazley, L., Kenchington, E., Koutsouveli, V., and Riesgo, A.: Cooperation between passive and active silicon transporters clarifies the ecophysiology and evolution of biosilicification in sponges, *Science Advances*, 6, eaba9322, <https://doi.org/10.1126/sciadv.aba9322>, 2020a.
- Maldonado, M., Beazley, L., López-Acosta, M., Kenchington, E., Casault, B., Hanz, U., and Mienis, F.: Massive silicon utilization facilitated by a benthic-pelagic coupled feedback sustains deep-sea sponge aggregations, *Limnol Oceanogr*, Ino.11610, <https://doi.org/10.1002/lno.11610>, 2020b.
- 940 MATLAB: version 7.10.0 (R2010a), The MathWorks Inc., Natick, Massachusetts, 2010.
- McIntyre, F. D., Drewery, J., Eerkes-Medrano, D., and Neat, F. C.: Distribution and diversity of deep-sea sponge grounds on the Rosemary Bank Seamount, NE Atlantic, *Mar Biol*, 163, 143, <https://doi.org/10.1007/s00227-016-2913-z>, 2016.
- Meyer, H. K., Roberts, E. M., Rapp, H. T., and Davies, A. J.: Spatial patterns of arctic sponge ground fauna and demersal fish are detectable in autonomous underwater vehicle (AUV) imagery, *Deep Sea Research Part I: Oceanographic Research Papers*, 945 153, 103137, <https://doi.org/10.1016/j.dsr.2019.103137>, 2019.
- Miatta, M. and Snelgrove, P. V.R.: Benthic nutrient fluxes in deep-sea sediments within the Laurentian Channel MPA (eastern Canada): The relative roles of macrofauna, environment, and sea pen octocorals, *Deep Sea Research Part I: Oceanographic Research Papers*, 178, 103655, <https://doi.org/10.1016/j.dsr.2021.103655>, 2021.
- Michna, P. and Woods, M.: RNetCDF: Interface to “NetCDF” Datasets, 2019.
- 950 Mienis, F., Duineveld, G. C. A., Davies, A. J., Ross, S. W., Seim, H., Bane, J., and van Weering, T. C. E.: The influence of near-bed hydrodynamic conditions on cold-water corals in the Viosca Knoll area, Gulf of Mexico, *Deep Sea Research Part I: Oceanographic Research Papers*, 60, 32–45, <https://doi.org/10.1016/j.dsr.2011.10.007>, 2012.
- Morganti, T. M., Slaby, B. M., de Kluijver, A., Busch, K., Hentschel, U., Middelburg, J. J., Grotheer, H., Mollenhauer, G., Dannheim, J., Rapp, H. T., Purser, A., and Boetius, A.: Giant sponge grounds of Central Arctic seamounts are associated with extinct seep life, *Nat Commun*, 13, 638, <https://doi.org/10.1038/s41467-022-28129-7>, 2022.
- 955 Morrison, K. M., Meyer, H. K., Roberts, E. M., Rapp, H. T., Colaço, A., and Pham, C. K.: The First Cut Is the Deepest: Trawl Effects on a Deep-Sea Sponge Ground Are Pronounced Four Years on, *Frontiers in Marine Science*, 7, 2020.
- Müller, K. and Wickham, H.: *tibble: Simple Data Frames*, 2023.

- 960 Murillo, F., Kenchington, E., Tompkins, G., Beazley, L., Baker, E., Knudby, A., and Walkusz, W.: Sponge assemblages and predicted archetypes in the eastern Canadian Arctic, *Mar. Ecol. Prog. Ser.*, 597, 115–135, <https://doi.org/10.3354/meps12589>, 2018.
- Murillo, F. J., Muñoz, P. D., Cristobo, J., Ríos, P., González, C., Kenchington, E., and Serrano, A.: Deep-sea sponge grounds of the Flemish Cap, Flemish Pass and the Grand Banks of Newfoundland (Northwest Atlantic Ocean): Distribution and species composition, *Marine Biology Research*, 8, 842–854, <https://doi.org/10.1080/17451000.2012.682583>, 2012.
- 965 Myers, R. A., Akenhead, S. A., and Drinkwater, K.: The influence of Hudson Bay runoff and ice-melt on the salinity of the inner Newfoundland Shelf, *Atmosphere-Ocean*, 28, 241–256, <https://doi.org/10.1080/07055900.1990.9649377>, 1990.
- Neuwirth, E.: RColorBrewer: ColorBrewer Palettes, 2014.
- Newton, P. P., Lampitt, R. S., Jickells, T. D., King, P., and Boutle, C.: Temporal and spatial variability of biogenic particles fluxes during the JGOFS northeast Atlantic process studies at 47°N, 20°W, *Deep Sea Research Part I: Oceanographic Research Papers*, 41, 1617–1642, [https://doi.org/10.1016/0967-0637\(94\)90065-5](https://doi.org/10.1016/0967-0637(94)90065-5), 1994.
- 970 Pedersen, T. L.: patchwork: The Composer of Plots, 2019.
- Petrie, B., Akenhead, S. A., Lazier, J., and Loder, J.: The cold intermediate layer on the Labrador and Northeast Newfoundland Shelves, 1978–86, 1988.
- Pham, C. K., Murillo, F. J., Lirette, C., Maldonado, M., Colaço, A., Ottaviani, D., and Kenchington, E.: Removal of deep-sea sponges by bottom trawling in the Flemish Cap area: conservation, ecology and economic assessment, *Sci Rep*, 9, 15843, <https://doi.org/10.1038/s41598-019-52250-1>, 2019.
- 975 Pile, A. J. and Young, C. M.: The natural diet of a hexactinellid sponge: Benthic–pelagic coupling in a deep-sea microbial food web, *Deep Sea Research Part I: Oceanographic Research Papers*, 53, 1148–1156, <https://doi.org/10.1016/j.dsr.2006.03.008>, 2006.
- 980 Polunin; Feeding relationships in Mediterranean bathyal assemblages elucidated by stable nitrogen and carbon isotope data, *Mar Ecol Prog Ser*, 220, 13–23, 2001.
- Puerta, P., Johnson, C., Carreiro-Silva, M., Henry, L.-A., Kenchington, E., Morato, T., Kazanidis, G., Rueda, J. L., Urrea, J., Ross, S., Wei, C.-L., González-Irusta, J. M., Arnaud-Haond, S., and Orejas, C.: Influence of Water Masses on the Biodiversity and Biogeography of Deep-Sea Benthic Ecosystems in the North Atlantic, *Frontiers in Marine Science*, 7, 239, <https://doi.org/10.3389/fmars.2020.00239>, 2020.
- 985 R Core Team: R: A Language and Environment for Statistical Computing, 2019.
- Radax, R., Rattei, T., Lanzen, A., Bayer, C., Rapp, H. T., Urich, T., and Schleper, C.: Metatranscriptomics of the marine sponge *Geodia barretti*: tackling phylogeny and function of its microbial community, *Environmental Microbiology*, 14, 1308–1324, <https://doi.org/10.1111/j.1462-2920.2012.02714.x>, 2012.
- 990 Rivkin, R. B., Legendre, L., Deibel, D., Tremblay, J.-É., Klein, B., Crocker, K., Roy, S., Silverberg, N., Lovejoy, C., Mesplé, F., Romero, N., Anderson, M. R., Matthews, P., Savenkoff, C., Vézina, A., Therriault, J.-C., Wesson, J., Bérubé, C., and Ingram, R. G.: Vertical Flux of Biogenic Carbon in the Ocean: Is There Food Web Control?, *Science*, 272, 1163–1166, <https://doi.org/10.1126/science.272.5265.1163>, 1996.

- Rix, L., de Goeij, J. M., Mueller, C. E., Struck, U., Middelburg, J. J., van Duyl, F. C., Al-Horani, F. A., Wild, C., Naumann, M. S., and van Oevelen, D.: Coral mucus fuels the sponge loop in warm- and cold-water coral reef ecosystems, *Sci Rep*, 6, 18715, <https://doi.org/10.1038/srep18715>, 2016.
- 995 Roberts, E. M., Mienis, F., Rapp, H. T., Hanz, U., Meyer, H. K., and Davies, A. J.: Oceanographic setting and short-timescale environmental variability at an Arctic seamount sponge ground, *Deep Sea Research Part I: Oceanographic Research Papers*, 138, 98–113, <https://doi.org/10.1016/j.dsr.2018.06.007>, 2018.
- 1000 Robertson, L. M., Hamel, J.-F., and Mercier, A.: Feeding in deep-sea demosponges: Influence of abiotic and biotic factors, *Deep Sea Research Part I: Oceanographic Research Papers*, 127, 49–56, <https://doi.org/10.1016/j.dsr.2017.07.006>, 2017.
- Rooks, C., Fang, J. K.-H., Mørkved, P. T., Zhao, R., Rapp, H. T., Xavier, J. R., and Hoffmann, F.: Deep-sea sponge grounds as nutrient sinks: denitrification is common in boreo-Arctic sponges, *Biogeosciences*, 17, 1231–1245, <https://doi.org/10.5194/bg-17-1231-2020>, 2020.
- 1005 Roy, V., Iken, K., and Archambault, P.: Environmental Drivers of the Canadian Arctic Megabenthic Communities, *PLOS ONE*, 9, e100900, <https://doi.org/10.1371/journal.pone.0100900>, 2014.
- Ryan, J. A. and Ulrich, J. M.: *xts: eXtensible Time Series*, 2024.
- Schläppy, M.-L., Weber, M., Mendola, D., Hoffmann, F., and de Beer, D.: Heterogeneous oxygenation resulting from active and passive flow in two Mediterranean sponges, *Dysida avara* and *Chondrosia reniformis*, *Limnology and Oceanography*, 55, 1289–1300, <https://doi.org/10.4319/lo.2010.55.3.1289>, 2010.
- 1010 Seers, B. and Shears, N.: *New Zealand's Climate Data in R — An Introduction to clifro*, The University of Auckland, Auckland, New Zealand, 2015.
- Sherwood, O. A., Heikoop, J. M., Scott, D. B., Risk, M. J., Guilderson, T. P., and McKinney, R. A.: Stable isotopic composition of deep-sea gorgonian corals *Primnoa* spp.: a new archive of surface processes, *Marine Ecology Progress Series*, 301, 135–148, <https://doi.org/10.3354/meps301135>, 2005.
- 1015 Sherwood, O. A., Jamieson, R. E., Edinger, E. N., and Wareham, V. E.: Stable C and N isotopic composition of cold-water corals from the Newfoundland and Labrador continental slope: Examination of trophic, depth and spatial effects, *Deep Sea Research Part I: Oceanographic Research Papers*, 55, 1392–1402, <https://doi.org/10.1016/j.dsr.2008.05.013>, 2008.
- Sherwood, O. A., Davin, S. H., Lehmann, N., Buchwald, C., Edinger, E. N., Lehmann, M. F., and Kienast, M.: Stable isotope ratios in seawater nitrate reflect the influence of Pacific water along the northwest Atlantic margin, *Biogeosciences*, 18, 4491–4510, <https://doi.org/10.5194/bg-18-4491-2021>, 2021.
- 1020 Shimeta, J. and Jumars, P. A.: Physical mechanisms and rates of particle capture by suspension feeders, *Oceanogr. Mar. Biol. Annu. Rev.*, 191–257, 1991.
- Shumway, R. H., Stoffer, D. S., and Stoffer, D. S.: *Time series analysis and its applications*, Springer, 2000.
- 1025 Sigman, D. M., Karsh, K. L., and Casciotti, K. L.: Nitrogen Isotopes in the Ocean, in: *Encyclopedia of Ocean Sciences*, Elsevier Ltd, 40–54, <https://doi.org/10.1016/B978-012374473-9.00632-9>, 2009.
- signal developers: *signal: Signal processing*, 2014.

- Smith, E. J., Soule, F. M., and Mosby, O.: The Marion and General Greene expeditions to Davis Strait and Labrador Sea., U.S. Coast Guard Bull., 19, 1937.
- 1030 Stoffer, D.: *astsa: Applied Statistical Time Series Analysis*, 2020.
- Straneo, F. and Saucier, F.: The outflow from Hudson Strait and its contribution to the Labrador Current, *Deep Sea Research Part I: Oceanographic Research Papers*, 55, 926–946, <https://doi.org/10.1016/j.dsr.2008.03.012>, 2008.
- Sutcliffe, W. H. Jr., Loucks, R. H., Drinkwater, K. F., and Coote, A. R.: Nutrient Flux onto the Labrador Shelf from Hudson Strait and its Biological Consequences, *Can. J. Fish. Aquat. Sci.*, 40, 1692–1701, <https://doi.org/10.1139/f83-196>, 1983.
- 1035 Thomson, D. H.: Marine Benthos in the Eastern Canadian High Arctic: Multivariate Analyses of Standing Crop and Community Structure, *Arctic*, 35, 61–74, 1982.
- Tremblay, J.-É., Gratton, Y., Carmack, E. C., Payne, C. D., and Price, N. M.: Impact of the large-scale Arctic circulation and the North Water Polynya on nutrient inventories in Baffin Bay, *Journal of Geophysical Research: Oceans*, 107, 26-1-26–14, <https://doi.org/10.1029/2000JC000595>, 2002.
- 1040 Turner, J. T.: Zooplankton fecal pellets, marine snow, phytodetritus and the ocean’s biological pump, *Progress in Oceanography*, 130, 205–248, <https://doi.org/10.1016/j.pocean.2014.08.005>, 2015.
- Vacelet, J. and Donadey, C.: Electron microscope study of the association between some sponges and bacteria, *Journal of Experimental Marine Biology and Ecology*, 30, 301–314, [https://doi.org/10.1016/0022-0981\(77\)90038-7](https://doi.org/10.1016/0022-0981(77)90038-7), 1977.
- 1045 Vander Zanden, M. J. and Rasmussen, J. B.: Variation in $\delta^{15}\text{N}$ and $\delta^{13}\text{C}$ trophic fractionation: Implications for aquatic food web studies, *Limnology and Oceanography*, 46, 2061–2066, <https://doi.org/10.4319/lo.2001.46.8.2061>, 2001.
- Vaughan, D. and Dancho, M.: *tibblertime: Time Aware Tibbles*, 2020.
- Vieira, R. P., Bett, B. J., Jones, D. O. B., Durden, J. M., Morris, K. J., Cunha, M. R., Trueman, C. N., and Ruhl, H. A.: Deep-sea sponge aggregations (*Pheronema carpensteri*) in the Porcupine Seabight (NE Atlantic) potentially degraded by demersal fishing, *Progress in Oceanography*, 183, 102189, <https://doi.org/10.1016/j.pocean.2019.102189>, 2020.
- 1050 Vogel, S.: Current-induced flow through living sponges in nature., *Proceedings of the National Academy of Sciences*, 74, 2069–2071, <https://doi.org/10.1073/pnas.74.5.2069>, 1977.
- White, M.: Comparison of near seabed currents at two locations in the Porcupine Sea Bight—implications for benthic fauna, *Journal of the Marine Biological Association of the United Kingdom*, 83, 683–686, <https://doi.org/10.1017/S0025315403007641h>, 2003.
- 1055 Whitney, F., Conway, K., Thomson, R., Barrie, V., Krautter, M., and Mungov, G.: Oceanographic habitat of sponge reefs on the Western Canadian Continental Shelf, *Continental Shelf Research*, 25, 211–226, <https://doi.org/10.1016/j.csr.2004.09.003>, 2005.
- Wickham, H.: Reshaping Data with the reshape Package, *Journal of Statistical Software*, 21, 1–20, 2007.
- Wickham, H.: *ggplot2: Elegant Graphics for Data Analysis*, Springer-Verlag New York, 2016.
- 1060 Wickham, H. and Bryan, J.: *readxl: Read Excel Files*, 2019.

- Wilke, C. O.: cowplot: Streamlined Plot Theme and Plot Annotations for “ggplot2,” 2019.
- Wilkinson, C. R., Garrone, R., Vacelet, J., and Smith, D. C.: Marine sponges discriminate between food bacteria and bacterial symbionts: electron microscope radioautography and in situ evidence, *Proceedings of the Royal Society of London. Series B. Biological Sciences*, 220, 519–528, <https://doi.org/10.1098/rspb.1984.0018>, 1984.
- 1065 Witte, U., Brattegard, T., Graf, G., and Springer, B.: Particle capture and deposition by deep-sea sponges from the Norwegian-Greenland Sea, *Marine Ecology Progress Series*, 154, 241–252, <https://doi.org/10.3354/meps154241>, 1997.
- Wu, Y., Peterson, I. K., Tang, C. C. L., Platt, T., Sathyendranath, S., and Fuentes-Yaco, C.: The impact of sea ice on the initiation of the spring bloom on the Newfoundland and Labrador Shelves, *Journal of Plankton Research*, 29, 509–514, <https://doi.org/10.1093/plankt/fbm035>, 2007.
- 1070 Wurz, E., Beazley, L., MacDonald, B., Kenchington, E., Rapp, H. T., and Osinga, R.: The Hexactinellid Deep-Water Sponge *Vazella pourtalesii* (Schmidt, 1870) (Rossellidae) Copes With Temporarily Elevated Concentrations of Suspended Natural Sediment, *Front. Mar. Sci.*, 8, <https://doi.org/10.3389/fmars.2021.611539>, 2021.
- Xie, Y.: knitr: A General-Purpose Package for Dynamic Report Generation in R, 2020.
- 1075 Yahel, G., Whitney, F., Reiswig, H. M., Eerkes-Medrano, D. I., and Leys, S. P.: In situ feeding and metabolism of glass sponges (Hexactinellida, Porifera) studied in a deep temperate fjord with a remotely operated submersible, *Limnol. Oceanogr.*, 52, 428–440, <https://doi.org/10.4319/lo.2007.52.1.0428>, 2007.
- Yashayaev, I.: Hydrographic changes in the Labrador Sea, 1960–2005, *Progress in Oceanography*, 73, 242–276, <https://doi.org/10.1016/j.pocean.2007.04.015>, 2007.
- 1080 Yashayaev, I.: Intensification and shutdown of deep convection in the Labrador Sea were caused by changes in atmospheric and freshwater dynamics, *Commun Earth Environ*, 5, 1–23, <https://doi.org/10.1038/s43247-024-01296-9>, 2024.
- Yashayaev, I. and Loder, J. W.: Further intensification of deep convection in the Labrador Sea in 2016, *Geophysical Research Letters*, 44, 1429–1438, <https://doi.org/10.1002/2016GL071668>, 2017.